AGU PUBLICATIONS

JGR

Journal of Geophysical Research: Solid Earth

RESEARCH ARTICLE
10.1002/2014JB011258

Key Points:
- A thermodynamically consistent theory of poroviscoelastoplasticity is developed
- Effective mechanical properties of poroviscoelastoplastic materials are proposed
- Bulk rheology shows decompaction weakening and an exponential creep law

Correspondence to:
V. M. Yarushina,
viktoriya.yarushina@ife.no

Citation:
Yarushina, V. M., and Y. Y. Podladchikov (2015), (De)compaction of porous viscoelastoplastic media: Model formulation, *J. Geophys. Res. Solid Earth*, *120*, 4146–4170, doi:10.1002/2014JB011258.

Received 6 MAY 2014
Accepted 10 MAY 2015
Accepted article online 29 MAY 2015
Published online 29 JUN 2015

(De)compaction of porous viscoelastoplastic media: Model formulation

Viktoriya M. Yarushina[1] and Yuri Y. Podladchikov[2]

[1]Institute for Energy Technology, Kjeller, Norway, [2]Institut des Sciences de la Terre, University of Lausanne, Lausanne, Switzerland

Abstract A nonlinear viscoelastoplastic theory is developed for porous rate-dependent materials filled with a fluid in the presence of gravity. The theory is based on a rigorous thermodynamic formalism suitable for path-dependent and irreversible processes. Incremental evolution equations for porosity, Darcy's flux, and volumetric deformation of the matrix represent the simplest generalization of Biot's equations. Expressions for pore compressibility and effective bulk viscosity are given for idealized cylindrical and spherical pore geometries in an elastic-viscoplastic material with low pore concentration. We show that plastic yielding around pores leads to decompaction weakening and an exponential creep law. Viscous and plastic end-members of our model are consistent with experimentally verified models. In the poroelastic limit, our constitutive equations reproduce the exact Gassmann's relations, Biot's theory, and Terzaghi's effective stress law. The nature of the discrepancy between Biot's model and the True Porous Media theory is clarified. Our model provides a unified and consistent formulation for the elastic, viscous, and plastic cases that have previously been described by separate "end-member" models.

1. Introduction

Fluid flow in porous media has received much attention over the last century [*Biot*, 1941, 1962; *Frenkel*, 1944; *Gassmann*, 1951; *Mckenzie*, 1984; *Scott and Stevenson*, 1984; *Sleep*, 1974; *Turcotte and Ahern*, 1978; *von Terzaghi*, 1923]. The theory of poroelasticity in the form proposed by *Biot* [1941, 1956a, 1956b, 1962] is widely used in the prediction of seismic wave propagation and has broad industrial applications that lie far beyond the originally proposed field of applications. The viscous model formulated by *Mckenzie* [1984] forms the basis for the understanding of sedimentary compaction and melt migration in partially molten rocks. In recent years, new extensions to the theory of fluid-saturated porous media based on rigorous thermodynamic constitutive modeling have appeared [*Bercovici et al.*, 2001; *Coussy*, 2004; *de Boer*, 2000; *Delacruz et al.*, 1993; *Gray and Miller*, 2005; *Lopatnikov and Cheng*, 2004; *Sramek et al.*, 2007; *Wilmanski*, 2006]. Most of these studies were restricted to the case of either reversible elastic or irreversible, but linear viscous, rheologies. However, mechanical compaction in porous media may include nonlinear irreversible and path-dependent processes that result from grain crushing, friction, and pore collapse [*Aydin and Johnson*, 1983; *Fortin et al.*, 2007; *Vajdova et al.*, 2004].

Nonlinear (elasto-)viscoplastic models are widely used for metals and other nonporous materials [*Hill*, 1950]. For porous materials, macro- and microscale nonlinear theories were proposed in the works of several authors [*Carroll and Holt*, 1972; *Coussy*, 2004; *Duva and Hutchinson*, 1984; *Green*, 1972; *Gurson*, 1977; *Perzyna and Drabik*, 1989; *Tvergaard*, 1981]. Due to imperfections in internal structure, rocks and many polycrystalline materials possess different properties in tension and compression [*Connolly and Podladchikov*, 2007; *Lyakhovsky and Hamiel*, 2007; *Lyakhovsky et al.*, 1993, 1997; *Nguyen et al.*, 2011]; they exhibit a difference in loading/unloading behavior and elastic hysteresis even at very small strains (on the order of 10^{-7}) typical for acoustic waves [*Johnson and Rasolofosaon*, 1996; *Kadish et al.*, 1996; *Mashinskii*, 2003; *Yarushina and Podladchikov*, 2010]. Mechanical compaction may be accompanied by dissolution processes [*Karcz et al.*, 2008]. Accounting for these nonlinearities and path dependency requires model verification for thermodynamic consistency [*Houlsby and Puzrin*, 2000].

In this paper, we present a simple mathematical model for nonlinear porous viscoelastoplastic materials. Our main motivation is to establish a simple unifying theory for porous fluid flow in a deformable matrix that is able to capture the range of rheological responses expected within the Earth's lithosphere. These responses

Table 1. List of Principal Notation

Symbol	Meaning	Unit
a, b, c	internal and external radii of RVE, plastic radius	m
g_i	gravitational force	m s^{-2}
G	elastic shear modulus of solid mineral grains	Pa
K_s, K_f	solid and fluid bulk moduli	Pa
K_d, K_u	drained and undrained bulk moduli	Pa
$K_{\text{pore}}, K_\varphi$	effective bulk moduli of pore space	Pa
m	$m = 1$ for cylindrical pores, $m = 2$ for spherical pores	
p^s, p^f	pressure of solid and fluid phases	Pa
v_i^s, v_i^f	solid and fluid velocity	m s^{-1}
U_i^s, U_i^f	solid and fluid displacements	m
Y	yield stress/cohesion	Pa
δ_{ij}	Kronecker-delta	
φ	porosity	
ϕ, ψ	internal angle of friction, angle of dilation	
$\eta_s, \eta_f, \eta_\varphi$	solid and fluid shear viscosity; effective viscosity	Pa s
ξ	$\xi = 1$ for compaction, $\xi = -1$ for decompaction	
ρ^s, ρ^f	solid and fluid density	kg m^{-3}
ω	aspect ratio of elliptical and spheroidal pores	

can vary from elastic small strain consolidation [*Biot*, 1941; *von Terzaghi*, 1923] to plastic porosity collapse from tenths to a few percents of porosity in near-surface sediments and up to high-temperature creep during extraction of melts and metamorphic fluids [*Connolly and Podladchikov*, 1998, 2000, 2007, 2013; *Keller et al.*, 2013]. Moreover, recent discovery of a continuum spectrum of the episodic tremor and slip events bridging the gap between slow tectonic motion and earthquakes [*Peng and Gomberg*, 2010] have created a need for two-phase mathematical models that are capable of episodic transitions from elastic loading to failure and stable creep.

The Maxwell model is a standard choice for viscoelastic lithosphere response at mantle convection time scales [*Beuchert and Podladchikov*, 2010] that is compatible with elastic deformation at the shorter postglacial rebound and with melt extraction time scales. We present a macroscopic Maxwell-type viscoelastic (de)compaction rheological model as an appropriate manifestation of pore-scale Maxwell viscoelasticity of the solid grains. We show that pore-scale plastic yielding around stress concentrators may be accounted for by the nonlinearity of the effective macroscopic (de)compaction viscosity [*Sonder and England*, 1986]. We verify thermodynamic admissibility of our model using classical irreversible thermodynamics. Our constitutive relations are consistent with Biot's poroelasticity, exact Gassmann's relations [*Gassmann*, 1951; *Gurevich*, 2007], and an effective stress law [*Nur and Byerlee*, 1971; *von Terzaghi*, 1923] that has been suggested and experimentally verified for poroelastic materials. We make use of the mathematical similarity in the description of viscous and elastic behavior at the microscale to infer the viscous limit of the macroscopic equations.

2. Thermodynamically Admissible Closed System of Equations

The system of equations describing fluid flow in porous viscoelastoplastic media can be formed on a basis of balance laws for fluid and solid phases (see Appendix A for detailed derivations and Tables 1 and 2 for notations used). It consists of conservation of linear momentum for both phases

$$\nabla_j\left(\overline{\tau}_{ij} - \overline{p}\delta_{ij}\right) - g_i\overline{\rho} = 0 \tag{1}$$

$$q_i^D = -\frac{k}{\eta_f}\left(\nabla_i p^f + g_i\rho^f\right) \tag{2}$$

and conservation of mass for both phases

$$\frac{1}{\rho^s}\frac{d^s\rho^s}{\mathrm{d}t} - \frac{1}{1-\varphi}\frac{d^s\varphi}{\mathrm{d}t} + \nabla_j v_j^s = 0 \tag{3}$$

$$\frac{\varphi}{\rho^f}\frac{d^f\rho^f}{\mathrm{d}t} + \frac{d^s\varphi}{\mathrm{d}t} + \varphi\nabla_j v_j^s + \nabla_j q_j^D = 0. \tag{4}$$

The Maxwell viscoelastic relationship [*Beuchert and Podladchikov*, 2010] relates deviatoric stresses and velocity gradients

$$\nabla_i v_j^s + \nabla_j v_i^s = \frac{1}{G}\frac{d^\nabla\overline{\tau}_{ij}}{\mathrm{d}t} + \frac{\overline{\tau}_{ij}}{\eta_s} \tag{5}$$

Table 2. Shorthand Notations

Symbol	Meaning
α	Biot-Willis coefficient, equation (12)
ε_{ij}	$=\left(\nabla_j v_i^s+\nabla_i v_j^s\right)/2-\nabla_k v_k^s\delta_{ij}/3$, deviator of strain rate
κ	$=(1-\xi\sin\phi)/(1+\xi\sin\phi)$, shorthand notation
$\overline{\rho}$	$=\rho^f\varphi+\rho^s(1-\varphi)$, total density
$\overline{\tau}_{ij}$	$=\tau_{ij}^s(1-\varphi)+\tau_{ij}^f\varphi$, total stress deviator
B	Skempton's coefficient, equation (13)
$\overline{p}$	$=p^f\varphi+p^s(1-\varphi)$, total pressure
p_e	$=\overline{p}-p^f=\left(p^s-p^f\right)(1-\varphi)$, effective pressure
q_i^D	$=\varphi\left(v_i^f-v_i^s\right)$, Darcy's flux
Y^*	$=2Y\xi\cos\phi/(1+\xi\sin\phi)$, shorthand notation
$\frac{\mathrm{d}^f}{\mathrm{d}t}$	$=\frac{\partial}{\partial t}+v_i^f\nabla_i=\frac{d^s}{dt}+\left(v_i^f-v_i^s\right)\nabla_i$, Lagrangian derivative with respect to fluid
$\frac{\mathrm{d}^s}{\mathrm{d}t}$	$=\frac{\partial}{\partial t}+v_i^s\nabla_i$, Lagrangian derivative with respect to solid
$\frac{\mathrm{d}^\nabla\sigma_{ij}}{\mathrm{d}t}$	$=\frac{\partial\sigma_{ij}}{\partial t}-\sigma_{ik}W_{kj}-\sigma_{jk}W_{ki}$, Jaumann objective stress rate
W_{ki}	$=\frac{1}{2}\left(\frac{\partial v_k}{\partial x_i}-\frac{\partial v_i}{\partial x_k}\right)$, antisymmetric part of velocity gradient

where $d^\nabla\overline{\tau}_{ij}/dt$ is the Jaumann objective stress rate that satisfies the objectivity principle, i.e., does not depend on the frame of reference (see Table 2 for description). The Maxwell viscoelastic volumetric response for porosity evolution is

$$\frac{d^s\varphi}{dt}=\frac{1}{K_\varphi}\left(\frac{d^fp^f}{\mathrm{d}t}-\frac{d^s\overline{p}}{\mathrm{d}t}\right)+\frac{1}{\eta_\varphi}\left(p^f-\overline{p}\right), \tag{6}$$

and elastic compressibility for fluid and solid densities is expressed as follows:

$$\frac{K_f}{\rho^f}\frac{d^f\rho^f}{\mathrm{d}t}=\frac{d^fp^f}{\mathrm{d}t} \tag{7}$$

$$\frac{K_s}{\rho^s}\frac{d^s\rho^s}{dt}=\frac{1}{1-\varphi}\left(\frac{d^s\overline{p}}{dt}-\varphi\frac{d^fp^f}{dt}\right)\approx\frac{\partial p^s}{\partial t}. \tag{8}$$

Equations (1)–(8) constitute a closed system of equations for 16 unknowns (i.e., three velocities, three components of Darcy's flux, two pressures, five deviatoric stress components, two densities, and porosity; see Tables 1 and 2 for notations used). Thermodynamic admissibility of this system is verified in Appendix A. A more familiar form of poroviscoelastic equations is recovered by substituting equations (6) through (8) into mass balance to eliminate the time derivatives of densities and porosity:

$$\nabla_k v_k^s=-\frac{1}{K_d}\left(\frac{d^s\overline{p}}{\mathrm{d}t}-\alpha\frac{d^fp^f}{\mathrm{d}t}\right)-\frac{\overline{p}-p^f}{(1-\varphi)\eta_\varphi} \tag{9}$$

$$\nabla_k q_k^D=\frac{\alpha}{K_d}\left(\frac{d^s\overline{p}}{\mathrm{d}t}-\frac{1}{B}\frac{d^fp^f}{\mathrm{d}t}\right)+\frac{\overline{p}-p^f}{(1-\varphi)\eta_\varphi} \tag{10}$$

where

$$\frac{1-\varphi}{K_d}=\frac{1}{K_\varphi}+\frac{1}{K_s} \tag{11}$$

$$\alpha=1-\frac{K_d}{K_s} \tag{12}$$

$$B=\frac{\frac{1}{K_d}-\frac{1}{K_s}}{\frac{1}{K_d}-\frac{1}{K_s}+\varphi\left(\frac{1}{K_f}-\frac{1}{K_s}\right)}. \tag{13}$$

Linear elastic limits (infinite η_φ) of equations (9) and (10) are consistent with Biot's poroelasticity, the effective stress law formulated by *Nur and Byerlee* [1971], and Gassmann's relations between elastic bulk moduli (see Appendix B).

The incompressible (infinite K_s and K_f) elastic limit is as follows:

$$\nabla_k v_k^s=-\frac{1}{(1-\varphi)K_\varphi}\left(\frac{d^s\overline{p}}{\mathrm{d}t}-\frac{d^fp^f}{\mathrm{d}t}\right) \tag{14}$$

$$\nabla_k q_k^D=\frac{1}{(1-\varphi)K_\varphi}\left(\frac{d^s\overline{p}}{dt}-\frac{d^fp^f}{dt}\right). \tag{15}$$

Time integration of these equations at small strains yields Biot's linear poroelastic equations for the incompressible case:

$$\nabla_k U_k^s = -\frac{\overline{p} - p^f}{(1-\varphi)K_\varphi} \tag{16}$$

$$\nabla_k\left(\varphi\left(U_k^f - U_k^s\right)\right) = \frac{\overline{p} - p^f}{(1-\varphi)K_\varphi}. \tag{17}$$

Biot's macroscopic model was confirmed by a number of upscaling techniques applied to average (pore-) microscale elasticity [*Berryman*, 2005; *Gurevich*, 2007; *Lopatnikov and Cheng*, 2004; *Pride et al*., 1992]. The above incompressible limit of Biot's model is in agreement with the so-called Theory of Porous Media [*Schanz*, 2009; *Schanz and Diebels*, 2003]. Due to the analogy between slow incompressible viscous motion and elastic deformation [*Goodier*, 1936], the following equations would be derived by the same techniques for the viscous pore(micro)-scale deformation:

$$\nabla_k v_k^s = -\frac{\overline{p} - p^f}{(1-\varphi)\eta_\varphi} \tag{18}$$

$$\nabla_k q_k^D = \nabla_k\left(\varphi\left(v_k^f - v_k^s\right)\right) = \frac{\overline{p} - p^f}{(1-\varphi)\eta_\varphi}. \tag{19}$$

Equations (9) and (10) are the simplest (Maxwell viscoelastic) addition to the elastic (equations (14) and (15)) and viscous (equations (18) and (19)) bulk deformation modes. They represent macroscopic manifestation of the microscopic (pore scale) Maxwell viscoelastic bulk and shear deformation.

3. Effective Pore Compressibility K_φ and Effective Viscosity η_φ

The compaction equations introduced above have two additional material parameters, pore compressibility K_φ and effective viscosity η_φ, that may depend on porosity and pore geometry. These parameters can be measured in experiments [*Dong et al*., 2010; *Zimmerman*, 1991] or derived theoretically based on effective media theory. The effective bulk modulus and the viscosity define the character of fluid flow through porous media. In particular, porosity waves are very sensitive to the functional dependence of effective viscosity on porosity and pressure. Depending on effective viscosity, they can take the form of spherical blobs, flattened ellipsoidal structures, or elongated tubular jets [*Connolly and Podladchikov*, 2013; V. M. Yarushina, et al., (De)compaction of porous viscoelastoplastic media: Solitary porosity waves, submitted to *Journal of Geophysical Research*, 2015]. Their size and speed of propagation are strongly influenced by effective viscosity. Even in standard industrial applications such as hydraulic fracturing, the structure of the effective bulk modulus influences the levels of fluid loss [*Yarushina et al*., 2013].

In this section, we derive the effective bulk modulus and the effective viscosity in viscoelastoplastic rocks containing idealized cylindrical or spherical pores (Figure 1). These two geometries capture different stages of compaction [*Wilkinson and Ashby*, 1975]. Spherical pores represent low-porosity material, while cylinders are well suited for intermediate porosities. The porous rock is then viewed as an assembly of irregular space-filling polygons with an internal cavity that might be idealized as cylindrical (spherical) shells with the specific ratio of radii determined by porosity so that

$$\varphi = (a/b)^{m+1}. \tag{20}$$

Parameter m takes values of 1 or 2 for cylindrical and spherical pores, respectively. Differentiation of equation (20) leads to a more practical rate form of the porosity equation:

$$\dot{\varphi}/(\varphi(m+1)) = v_r/r|_{r=a} - v_r/r|_{r=b} \tag{21}$$

where v_r is the rate at which the walls of the shell contract or expand. Changes in total and fluid pressures in the porous rock cause changes in the size of each shell and hence in porosity. We assume that each of the shells forms a representative volume element (RVE), i.e., it deforms (1) independently of the other shells and (2) similar to all other shells. In addition, porosity is assumed to be sufficiently small so that interaction

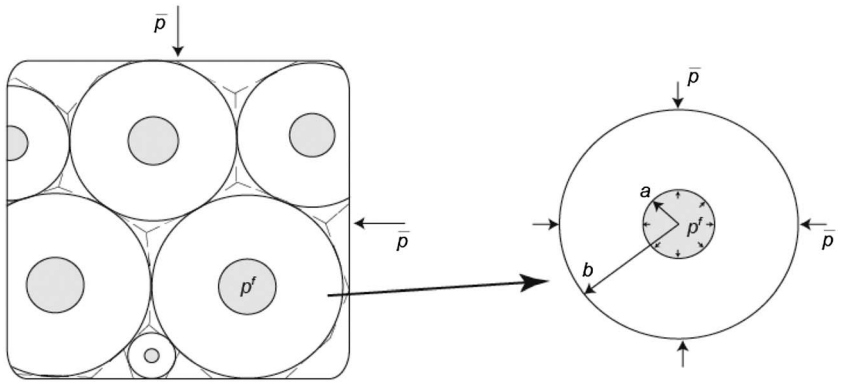

Figure 1. Viscous (elastic) model of porous media. A solid matrix contains cylindrical (spherical) pores of different sizes. Each pore of radius a is surrounded by a solid deformable shell of radius b. For elastic deformation of a shell, the rates of fluid pressure $\dot{p}^f$ and total pressure $\dot{\bar{p}}$ are prescribed at the internal and external boundaries of the shell, respectively. The elastic properties of the shell are the same as of the rock mineral grains and are given by bulk modulus K_s and shear modulus G_s. For viscous deformation, inside every pore there is uniform pore pressure p^f. The outer wall of the shell is subjected to a uniform total pressure $\bar{p}$. The bulk and shear viscosities of the shell are ζ_s and η_s.

between different pores is ignored. A solid matrix is composed of minerals with similar mechanical properties that do not swell or shrink in the presence of saturating fluid. Thus, by considering the mechanical equilibrium of one shell under an applied load, we find a rate at which the pore space contracts or expands, i.e., the porosity equation.

One of the fundamental questions related to the concept of an RVE is the correct formulation of the pressure boundary conditions on the inner and outer walls of the shell, given that at least four pressures are associated with the porous rocks, namely, p^f, p^s, $\bar{p}$, and p_e. In our model, we impose p^f on the pore boundary and $\bar{p}$ on the outer boundary (see Appendix C for detailed discussion). Compaction equations obtained by volume averaging are consistent with thermodynamically derived viscous compaction equations and with exact Gassmann's relations in the elastic limit.

3.1. Viscoelasticity

At low stresses and high strain rates, rocks exhibit elastic behavior. In sedimentary rocks, pressure solution on grain boundaries in the presence of fluids leads to viscous deformation. Deeper in the Earth, the cold upper mantle deforms by diffusion creep at a relatively low stress level [*Karato*, 2008] and also results in a linear viscous rheology. The solution to elastic and viscous boundary value problems discussed in detail in Appendix C gives the radial velocity of the shell as a function of total and fluid pressures. Using boundary velocities in equation (21) leads to the following elastic porosity equation:

$$\dot{p}_e = -K_\varphi \dot{\varphi} \tag{22}$$

and the following viscous porosity equation:

$$p_e = -\eta_\varphi \dot{\varphi} \tag{23}$$

with

$$K_\varphi = \frac{2m}{m+1}\frac{G}{\varphi}, \quad \eta_\varphi = \frac{2m}{m+1}\frac{\eta_s}{\varphi}. \tag{24}$$

Mechanical equilibrium in elastic and viscous materials has a similar description. This fact is largely known as the correspondence principle. It is responsible for similarity between derived elastic and viscous porosity equations.

3.2. Viscoplasticity

Elevated temperatures and the presence of pore fluids reduce the strength of the rock. Local heterogeneities such as pores, edges, or grain boundaries have the ability to amplify stresses locally. The combination of these factors can eventually lead to the development of a permanent plastic deformation around structural imperfections. Unlike viscous deformation, which is also permanent but rate dependent, plastic deformation

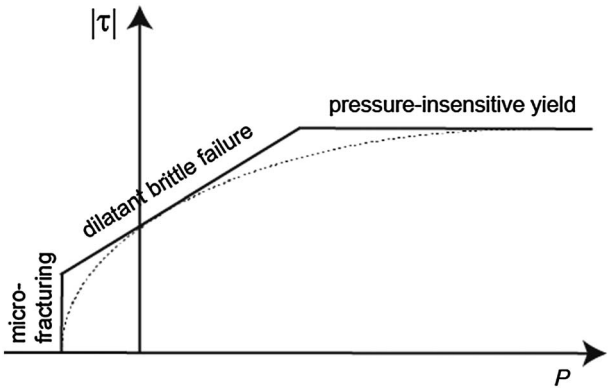

Figure 2. Typical nonlinear failure curve (dotted line) and its piecewise linear approximation (solid line) used as a microscopic yield criterion for plastic flow around pores.

is rate independent and occurs only when stresses reach a certain yield criterion. Viscous, elastic, and plastic deformation can develop simultaneously allowing materials to flow like viscous fluids at very long time scales and yet sustain the propagation of seismic waves at short time scales.

We consider three different types of plastic deformation: (1) dilatant brittle failure associated with frictional sliding on grain boundaries; (2) pressure-insensitive, nondilatant failure associated with deformation accommodated by mode II shear microcracks or crystal plasticity; and (3) generation of mode I open microfractures in an extensional regime (Figure 2). These modes correspond to three different stress levels. Dilatant brittle failure is expected to occur in crustal and upper mantle rocks that deform under moderate stress and low-temperature conditions [*Escartin et al*., 1997; *Hirth*, 2002; *Karato*, 2008]. The increasing confining pressure with depth tends to reduce frictional sliding of crack surfaces. Observations [*Escartin et al*., 1997; *Hirth*, 2002] indicate that high-pressure samples are brittle, but mode II shear cracks dominate with increasing pressure and lead to significant deviations from Byerlee's law. We interpret the reduction of the pressure dependence of the yield stress at high pressures observed in experiments as a transition from Mohr-Coulomb plasticity to von Mises yielding. Microfracturing is expected for tensile loads (Figure 2). In the deep Earth, brittle deformation is replaced by viscous ductile flow. However, before this happens, viscous flow and brittle failure act together in a transitional semibrittle regime. This regime is characterized by high stresses, weak temperature dependence, and exponential dependence of strain rate on stress that cannot be explained by linear diffusional or power law dislocation creep [*Karato*, 2008]. We show on a theoretical basis that pressure-insensitive yielding leads to exponential dependence of strain rate on stress, while dilatant brittle failure and microfracturing lead to different rheological behavior in compaction and decompaction regimes.

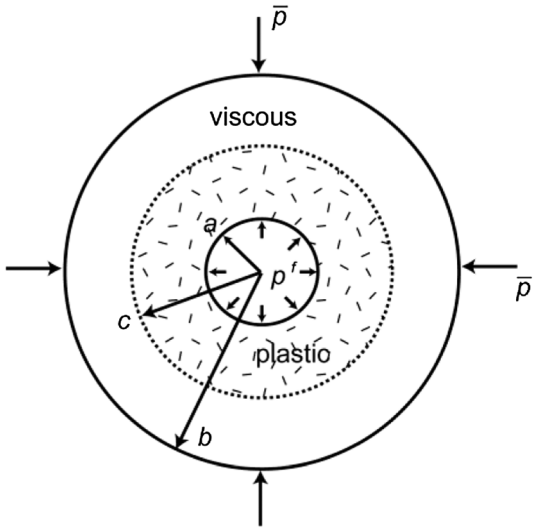

Figure 3. Viscoplastic cylindrical (spherical) model of a representative volume element subjected to total pressure $\overline{p}$ and fluid pressure p^f. In response to external loads that reached a certain yield criterion, the plastic domain of radius c spreads into the shell from the inner boundary. The rest of the volume is still in a viscous state. The viscous volumetric deformation of the shell walls is assumed to be negligible in comparison to shear viscosity ($\zeta_s = 0$).

In porous materials, plastic yielding concentrates around pores (Figure 3). Before the onset of plasticity, the material behavior is viscous. As stresses around the pore increase in response to rising effective pressure, the plastic region of radius c starts to grow. Viscous flow continues further away from the plastic boundary. The nucleation of the first kern of plasticity marks the onset of pore collapse with the critical pressure determined by microscale failure criterion. From that time on, increasing load leads to the growth of plastic zones until the plastic radius c reaches the outer boundary of an RVE. That moment corresponds to the full plastic pore collapse when the whole rock is in failure. Plastic flow around the pore reduces the stress concentration and enhances compaction or decompaction in comparison with a purely elastic or viscous case.

3.2.1. Pressure-Insensitive Yielding

Pressure-insensitive nondilatant failure is associated with Tresca or von Mises yield criteria on the pore

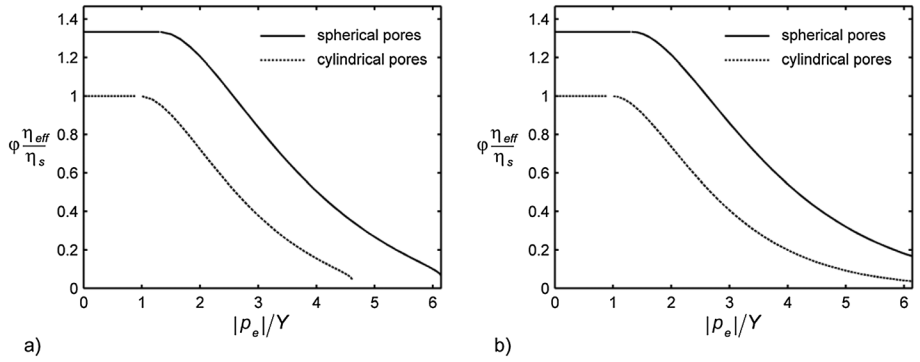

Figure 4. Effective viscosity η_φ of a pressure-insensitive viscoplastic porous rock normalized to the shear viscosity of the solid rock frame η_s and porosity φ as a function of ratio $|p_e|/Y$ of the absolute value of effective pressure to the yield strength of rock frame. (a) Effective viscosity is calculated according to equation (26) at $\varphi = 0.01$ for cylindrical and spherical pores. (b) The small porosity approximation to effective viscosity is calculated according to equation (28) for cylindrical and spherical pores. Both exact and approximate trends show that cylindrical pores are more compliant; however, the effect of pore geometry on effective viscosity is rather weak. Plastic yielding reduces the effective viscosity. Ductile plastic deformation does not make a difference in compactive versus decompactive behavior of a porous rock.

scale. Both of them give the following range of effective pressures at which viscoplastic compaction in ductile porous materials occurs (see Appendix D for derivations):

$$1-\varphi \le \frac{m+1}{2m}\frac{|p_e|}{Y} \le \ln 1/\varphi. \tag{25}$$

The lower limit in equation (25) defines the onset of plasticity, and the upper bound stands for the full plastic pore collapse. Both critical pressures depend on porosity, which is a function of the current stress state. Therefore, macroscopic behavior exhibits hardening during compaction and softening during decompaction. At p_e satisfying equation (25), the porosity equation takes the form of equation (23) with effective viscosity depending on effective pressure, yield stress, pore geometry, and shear viscosity of a solid matrix

$$\eta_\varphi = \frac{\eta_s}{\varphi(1-\varphi)}\frac{|p_e|}{Y}(c/a)^{-m-1} \tag{26}$$

where c/a defines the size of the plastically flowing zone near the idealized pore and has the following dependence on p_e:

$$|p_e/Y| = 2m/(m+1)\cdot\left(1+\ln(c/a)^{m+1}-\varphi(c/a)^{m+1}\right). \tag{27}$$

In a small porosity limit ($\varphi << 1$), equation (26) reduces to

$$\eta_\varphi = \frac{\eta_s}{\varphi}\frac{|p_e|}{Y}\exp\left(1-\frac{|p_e|}{Y}\frac{m+1}{2m}\right). \tag{28}$$

Figure 4 shows the dependence of effective viscosity on effective pressure for nondilute and dilute porosity distributions calculated according to equations (26) and (28). Equation (28) gives an exponential flow law associated with the brittle-ductile transition and rock behavior at low temperatures [*Evans and Goetze*, 1979; *Karato*, 2008].

At full pore collapse corresponding to the upper limit in equation (25), the viscoplastic interface reaches the outer boundary of the shell, and the compaction of the entire porous matrix is fully plastic. The pore compaction relation for this phase of compaction relates the porosity directly to effective pressure:

$$p_e = 2m/(m+1)\cdot Y\xi\ln(1/\varphi). \tag{29}$$

The full pore collapse relation in equation (29) plays a role similar to the normal consolidation line in the elastoplastic Cam-Clay model [*Sheldon et al.*, 2006]. However, in viscoplastic models, the permanent deformation that develops below the critical pressure in equation (29) is rate dependent and can accumulate at constant stresses.

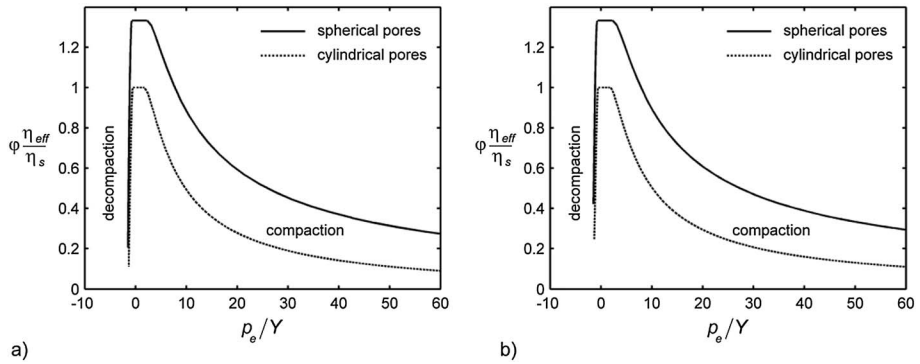

Figure 5. Effective viscosity η_φ of a brittle viscoplastic porous rock normalized to the shear viscosity of the solid rock frame η_s and porosity φ as a function of ratio p_e/Y of effective pressure to the yield strength of the rock frame. (a) Effective viscosity is calculated according to equation (31) at $\varphi = 0.01$ for cylindrical and spherical pores. (b) The small porosity approximation to effective viscosity is calculated according to equation (32) for cylindrical and spherical pores. All calculations are performed for a friction angle of $\psi = \pi/6$ and a dilation angle $\phi = 0$. Both exact and approximate trends show that cylindrical pores are more compliant; however, the effect of pore geometry on effective viscosity is rather weak. Plastic yielding reduces the effective viscosity. Brittle plastic deformation leads to decompaction weakening of a porous rock and shows different dependence of effective viscosity on effective pressure for compaction and decompaction.

3.2.2. Dilatant Brittle Failure

Brittle failure is associated with the Mohr-Coulomb yield criterion on the pore scale, which leads to the following pressure range for viscoplastic deformation (see Appendix D for details):

$$\frac{m}{\kappa(m+1)}(1-\varphi) \le \frac{p_e}{Y^*} \le \frac{1}{\kappa-1}\left(1-\varphi^{m(\kappa-1)/((m+1)\kappa)}\right). \tag{30}$$

The lower limit in equation (30) defines the plasticity onset, and the upper bound stands for the full plastic pore collapse. Similar to previous case of pressure-insensitive yielding, critical pressures in equation (30) depend on porosity, which accounts for hardening/softening behavior. In the viscoplastic regime, effective viscosity takes the following form:

$$\eta_\varphi = \frac{2\eta_s\kappa}{\varphi}\frac{p_e}{Y^*}\left(1-\varphi\widetilde{P}^{(\kappa+m)/(m-m\kappa)} + \frac{\left(\widetilde{P}^{\gamma}-1\right)(\kappa+m)}{m(1-\kappa)\gamma}\right)^{-1} \tag{31}$$

where

$$\gamma = 1-\kappa/(\kappa-1)\cdot(1/\varsigma+1/m)$$

$$\widetilde{P} = \kappa(m+1)(a/c)^{m+1}\frac{1+(1-\kappa)p_e/Y^*}{(a/c)^{m+1}(\kappa+m)+\varphi(\kappa-1)m}.$$

In a small porosity limit ($\varphi << 1$),

$$\eta_\varphi = \frac{2\eta_s\kappa}{\varphi}\frac{p_e}{Y^*}\left(1+\frac{\left(\widetilde{P}^{\gamma}-1\right)(\kappa+m)}{m(1-\kappa)\gamma}\right)^{-1} \tag{32}$$

with

$$\widetilde{P} = \frac{\kappa(m+1)}{(\kappa+m)}(1+(1-\kappa)p_e/Y^*).$$

In the plastic regime, effective viscosities in equations (31) and (32) for brittle viscoplastic porous materials are strongly dependent on the magnitude and the sign of effective pressure (Figure 5). Increasing load tends to reduce effective viscosity and significantly enhances viscous deformation. Dependence on the sign of loading results in the difference in the material response to tensile and compression loads so that an equal

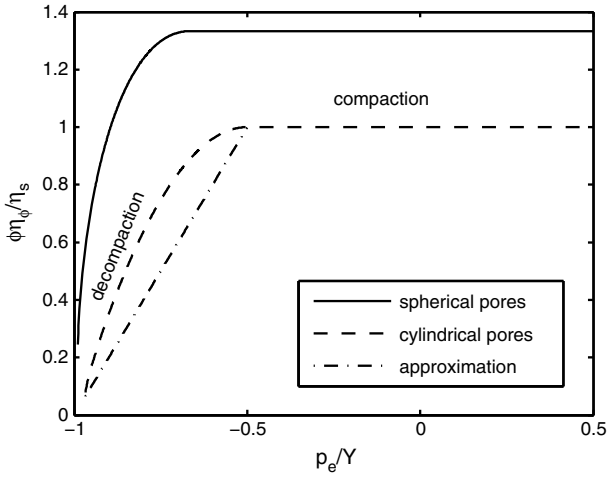

Figure 6. Effective viscosity η_φ of a viscoplastic porous rock with microfracturing normalized to the shear viscosity of the solid rock frame η_s and porosity φ as a function of ratio p_e/Y of effective pressure to the yield strength of the rock frame. Effective viscosity is calculated according to equations (34)–(36) at $\varphi = 0.001$ for cylindrical and spherical pores.

degree of decompaction would occur at much lower stresses than compaction (Figure 5). Accordingly, equal compressive and tensile stresses would result in the much higher rates of decompaction in comparison with compaction (i.e., decompaction weakening). When effective pressure reaches the upper limit in equation (30), the pore compaction relation for the fully plastic phase of compaction takes the following form:

$$p_e = \frac{Y^*}{\kappa - 1}\left(1 - \varphi^{m(\kappa-1)/((m+1)\kappa)}\right).$$

3.2.3. Microfracturing

At high fluid pressures or low total pressure, microfracturing might occur. In a rock with spherical or cylindrical pores, fractures emanate from the voids. Fracture growth on the pore scale is governed by the Griffith failure criterion [e.g., *Jaeger et al.*, 2007, pp. 314–320] according to which distributed microfracturing in porous rock occurs in the decompaction regime when (see Appendix D for detailed derivations)

$$-\left(1 - \varphi^{\frac{m}{m+1}}\right) \le \frac{p_e}{Y} \le -\frac{m(1-\varphi)}{m+1} \tag{33}$$

with effective viscosity of the form

$$\eta_\varphi = \frac{2\eta_s p_e}{(1-\varphi)\left(\sqrt{(p_e+Y)^2 - \varphi Y^2} - (p_e+Y)\right)} \tag{34}$$

for cylindrical pores and

$$\eta_\varphi = -\frac{2}{3}\frac{\eta_s p_e}{\varphi}\frac{(a/c)^3 + 2\varphi}{(p_e+Y)(1-\varphi)} \tag{35}$$

for spherical pores, where a/c ratio can be found from equation (D11). Compaction and the nonfracturing part of decompaction can be described with effective viscosity in equation (24) obtained for purely viscous deformation. At the point of full pore collapse given as a lower limit in equation (33), the effective viscosity is still finite (Figure 6), and its value depends on porosity and pore geometry:

$$\eta_\varphi = \frac{2\eta_s}{(1-\varphi)}\left(\varphi^{-\frac{m}{m+1}} - 1\right).$$

Even at small overpressures, microfracturing in rocks can reduce effective viscosity tenfold depending on the porosity. This leads to a strong asymmetry with respect to the sign of loading (Figure 6). Taking into account that decompaction weakening occurs in a narrow pressure interval and considering the uncertainties associated with the idealizations of the cylindrical (spherical) model, the use of complex relations for effective viscosity might not be justified. The nonlinear part of effective viscosity associated with microfracturing in a small porosity limit can well be approximated with a linear relationship (Figure 6):

$$\eta_\varphi \approx \frac{\eta_s}{\varphi}\begin{cases} 2(1+p_e/Y) & at \quad -\left(1-\sqrt{\varphi}\right) \le p_e < -Y/2 \\ 1 & at \quad p_e \ge -Y/2 \end{cases}. \tag{36}$$

Brittle-ductile deformation in rocks, whether due to dilatant brittle failure or microfracturing, leads to a difference in material response to compactive and dilating loads in the form of decompaction weakening.

Such a difference in compaction/decompaction viscosities was identified before as a reason for generating tubular fast-propagating high-porosity regions (i.e., porosity waves) that are able to efficiently transport fluids in the crust and upper mantle [*Connolly and Podladchikov*, 2013].

4. Comparison to the Previous Models

4.1. Poroelasticity

The field of finite-strain poroelasticity is still under development [*Coussy*, 1989; *Ehlers and Eipper*, 1999]. Therefore, we compare here our nonlinear constitutive equations to well-established theories for small strain. *Rice and Cleary* [1976] give linear poroelastic constitutive equations that can be represented in the form

$$v - v_0 = -(1/K_d - 1/K_s)p_e - v_0/K_s p^f \tag{37}$$

$$\overline{p} - \alpha p^f = -K_d \varepsilon \tag{38}$$

$$p^f = K_f\left(\rho^f - \rho_0^f\right)/\rho_0^f \tag{39}$$

where ε is the total volumetric deformation, and v is the apparent fluid volume fraction, i.e., the Lagrangian porosity that relates the pore volume to the total volume in the reference state ($v = V_p/V_0 = \varphi V/V_0$). Note that our fluid and solid equations of state in equations (7) and (9) reduce to equations (38) and (39) in the linear elastic case. Equation (37) is consistent with the elastic part of our porosity in equation (6) if Eulerian porosity is introduced as $d\varphi = dv - \varphi dV/V_0$. *Detournay and Cheng* [1993] and *Wang* [2000] give several different formulations of linear poroelastic constitutive in equations (37)–(39) and show that they are equivalent to Biot's poroelastic theory [*Biot*, 1941]. *Lopatnikov and Cheng* [2004] present nonlinear elastic constitutive equations that after linearization and certain assumptions on material homogeneity lead to linear equations (37)–(39). The linear poroelastic equations of *Carroll* [1980b], *Coussy* [2004], and *Guéguen et al*. [2004] are also consistent with equations (37)–(39).

Nonlinear elastic incremental state equations for small strains were previously formulated by *Carroll* [1980a], *Rice* [1975], and *Coussy* [2004]. It can be shown that the elastic parts of our equations (6), (9), and (10) are consistent with those of *Rice* [1975] and *Coussy* [2004]. They are also consistent with the constitutive equations of *Carroll* [1980b]. However, based on effective media theory, *Carroll* [1980b] derives a different relationship between bulk moduli that depends not only on porosity as in our equation (11) but also on effective pressure:

$$\frac{1-\varphi}{K_d} = \frac{1}{K_s} + \frac{1}{K_\varphi}\left(1 - \frac{\overline{p} - p^f}{(1-\varphi)K_s}\right). \tag{40}$$

Equation (40) follows from the porosity equation and equation of state for a solid matrix taken in the form

$$dp^s = -K_s dV_s/V_s. \tag{41}$$

However, in a porous rock, the solid matrix feels the presence of the second phase through porosity and fluid pressure. Therefore, the nonlinear macroscopic definition of solid bulk modulus given by equation (8) involves both total and fluid pressures.

The constitutive equations of the theory of True Porous Media were claimed to be different from Biot's equations [*de Boer*, 2000, p. 111]. The difference concerns the Biot factor that influences the volumetric response (K_d/K_s in equation (12)). To clarify this discrepancy, we rewrite the equation for the total volumetric deformation known as an effective stress law as predicted by both theories:

1. Biot's poroelasticity

$$\overline{p} - \alpha p^f = -K_d \varepsilon \tag{38}$$

$$\alpha = 1 - \frac{K_d}{K_s} \tag{12}$$

$$\frac{1-\varphi}{K_d} = \frac{1}{K_\varphi} + \frac{1}{K_s}; \tag{11}$$

2. Theory of true porous media

$$\overline{p} - \left(1 - B^S(1-\varphi)\right)p^f = -\hat{K}^S\varepsilon \tag{42}$$

$$B^S = \frac{K^{SN}}{K^{SR} + K^{SN}} \tag{43}$$

$$\hat{K}^S = (1-\varphi)K^{SR}B^S. \tag{44}$$

Equation (42) is based on equation (8.22) from *de Boer* [2000] for the case of purely volumetric deformation, where we rewrote porosity and pressures in our notations. Material parameters in equations (43) and (44) are taken from equations (8.20) and (8.21) from the same source. Indeed, equation (42) contains an effective stress coefficient $(1 - B^S(1-\varphi))$, which apparently looks different from the Biot-Willis parameter α given by equation (12). According to *de Boer* [2000], "quantity B^S […] is similar to the Biot factor […] with the difference being that the denominator in the Biot factor contains only the compression modulus of the real material K^{SR}, whereas in equation (8.20) (equation (42)), the denominator consists of the sum of the compression modulus of the real materials K^{SR} and the compression modulus of the solid skeleton K^{SN}. Only in the case where K^{SN} is very small in comparison with K^{SR} are both results approximately equal."

Moduli K^{SR} and K^{SN} are interpreted by *de Boer* [2000] as the bulk modulus of the real material (K_s in our notation) and the bulk modulus of the solid skeleton, respectively. The last definition is a little vague, since there are several bulk moduli that can be related to the skeleton, including K_d and K_φ. Obviously, de Boer compares his parameter K^{SN} to the drained bulk modulus K_d. To establish the true meaning of K^{SN}, we look at its definition given by equation (8.7) from *de Boer* [2000]

$$p_E^{SN} = K^{SN}e_{SN}. \tag{45}$$

Pressure p_E^{SN}, which was introduced by equation (8.5) in *de Boer* [2000], in our notations reads $p_E^{SN} = p^f - p^s$; e_{SN} is defined by de Boer as the volumetric strain due to the change of pores in size. By looking at equation (45), one can see that modulus K^{SN} is related to the compressibility of pore space rather than to the total deformation of the skeleton as assumed by de Boer. Thus, the following identities must be used for comparison of the two theories: $K^{SN} \equiv K_\varphi$ and $\hat{K}^S \equiv K_d$ as in equations (42) and (38). With these new definitions in mind, the effective stress coefficient in the true porous media becomes

$$1 - B^S(1-\varphi) = 1 - \frac{K_\varphi}{K_s + K_\varphi}(1-\varphi) = 1 - \frac{K_d}{K_s} = \alpha \tag{46}$$

where we made use of equation (11). Thus, the effective stress coefficient in constitutive equations of the theory of True Porous Media coincides exactly with the Biot-Willis coefficient in the effective stress law in equation (38). Moreover, equation (44), which serves as a definition of bulk modulus $\hat{K}^S$, is identical to our equation (11). The apparent discrepancy between Biot's constitutive equations and the linear constitutive equations of the theory of True Porous Media stems from the misinterpretation of material parameters K^{SN} and B^S introduced in the latter. Once the correction is made, both sets of constitutive equations become identical.

The theoretical bulk modulus for elastic materials with various pore geometries was derived in the works of *Christensen* [1979], *Budiansky and Oconnell* [1976], *Mackenzie* [1950], and many others. Some of the popular geometries include two-dimensional cracks of various shapes, spheroids (i.e., geometrical shapes obtained as a result of revolution of an ellipse about one of its axes that has two equal axes and one unequal axis of symmetry), and tubes with three- or four-sided cross sections in the form of a hypotrohoid (i.e., a geometrical shape with slightly concave sides and rounded corners) [*Mavko et al.*, 1998; *Zimmerman*, 1991]. As a rule, approximations are given for the effective bulk modulus K_{pore} (see equation (B7) of Appendix B for definition) related to our modulus K_φ as follows:

$$\frac{1-\varphi}{K_{\text{pore}}} = \frac{1}{\varphi K_\varphi} + \frac{1}{K_s}. \tag{47}$$

Summarizing results for K_{pore} from *Zimmerman* [1991] we can write

$$K_\varphi = \frac{G}{\varphi} \cdot \begin{cases} 2\left(\omega + \dfrac{1}{\omega}\right)^{-1} & \text{for elliptical tubular pores} \\ \dfrac{1 - n\lambda^2}{1 + n\lambda^2} & \text{for hypotrochoidal tubular pores} \\ \dfrac{2\omega^2 + \ln(4\omega^2)}{2\omega^2 + 1} & \text{for spheroidal pores,} \quad \omega > 2 \end{cases} \tag{48}$$

The incompressible case ($1/K_s = 0$) is chosen here for simplicity of mathematical expressions. Here ω is the ellipse (spheroid) aspect ratio. For elliptical tubular pores, it is defined as the ratio of the minor to major axis of symmetry so that $\omega \leq 1$ with $\omega = 1$ for circular cylinders and $\omega \to 0$ for very thin elliptical tubes. For spheroidal pores, ω is the ratio of unequal axis to the length of one of the equal axes of symmetry. In the limit $\omega = 1$, spheroidal pores become spheres. Values of $\omega \to 0$ correspond to very thin penny-shaped cracks, while $\omega \to \infty$ correspond to infinitely long needle-like cylinders. Parameter n is a positive integer equal to the number of corners in the hypotrochoidal pore minus one, and λ is a real number ($0 \leq \lambda < 1/n$) responsible for the roundness of corners. One can see that pores of very different geometries surprisingly all yield the same functional dependence of the bulk modulus on porosity. Differences in geometries result in a geometric factor after the leading term G/φ. Hypotrochoidal and spheroidal pores give geometric factors close to 1, while elliptical pores effectively decrease K_φ in comparison with the reference circular tubular pores considered in the previous sections. For instance, elliptical pores with an aspect ratio $\omega = 100$ lead to $\varphi K_\varphi = 0.015G$, which reduces the effective bulk modulus by 2 orders of magnitude. Therefore, we suggest a generalized form of the effective bulk modulus

$$K_\varphi = \widetilde{m}\frac{G}{\varphi} \tag{49}$$

in which the geometric factor $\widetilde{m}$ accounts for the variations in pore geometry and takes values between 4/3 for spheroidal pores and 2ω for very thin crack-like pores with aspect ratio $\omega \to 0$ (see also equation (48)). A similar geometric factor is used in several expressions for effective viscosity that we review in the next section.

4.2. Poroviscosity

To compare with viscous models, we note that in the purely viscous case, fluid and solid compressibility equations (7) and (8) are trivial, and the matrix compaction equation (9) yields

$$p^s - p^f = -\eta_\varphi \nabla_k v_k^s. \tag{50}$$

This equation is often used to explain compaction of partially molten rocks and magma ascent by porous flow [*Hewitt and Fowler*, 2008; *Mckenzie*, 1984; *Sumita et al*., 1996]. However, there are several thermodynamically admissible definitions of effective viscosity. One of them defines effective bulk viscosity, η_b, as the ratio between the effective pressure and volumetric deformation [*Schmeling*, 2000; *Stevenson and Scott*, 1991], i.e.,

$$p_e = \left(p^s - p^f\right)(1 - \varphi) = -\eta_b \nabla_k v_k^s. \tag{51}$$

The two effective viscosities η_b and η_ϕ are related through the following equation:

$$\eta_\varphi = \frac{\eta_b}{1 - \varphi}. \tag{52}$$

Viscosities η_b and η_φ are identical in a small porosity limit ($\varphi \ll 1$); however, care must be taken when comparing different expressions for bulk viscosities for nonnegligible porosities.

Knowledge about the porosity dependence of effective viscosity is important for understanding the fluid migration in porous media. Several different expressions have been proposed for the effective bulk viscosity in the literature. The major difference between them is in the functional form of the porosity dependence of effective viscosity. *Wilkinson and Ashby* [1975] and later *Carroll* [1980a], by considering spherical shells, obtained the effective viscosity in the form of equation (24) with $m = 4/3$. *Hewitt and Fowler* [2008], based on a microscopic cylindrical model, derived effective viscosity in the form of equation (24) with $m = 1$.

Recently, *Schmeling et al*. [2012] numerically derived effective shear and bulk viscosities in purely viscous rocks with singular cavities of various geometries. They showed that spherical and ellipsoidal inclusions lead to

$$\eta_b = c_1 \eta_s \frac{(c_2 - \varphi)^k}{\varphi} \tag{53}$$

where parameters c_1, c_2, and k depend on the melt geometry. For spherical melt pores, $c_1 = 4/3$, $c_2 = 1$, and $k = 1$ are proposed [*Schmeling*, 2000]. Conversion of η_b into η_φ results in equation (24) with $m = 4/3$. *Bercovici et al*. [2001], by considering infinitely long cylinders filled with a viscous fluid that supports shear stresses, obtained

$$\eta_\varphi = -\widetilde{m} \frac{\eta_s + \eta_f}{\varphi} \tag{54}$$

where $\widetilde{m}$ is a dimensionless geometry factor. *Sramek et al*. [2007] ignore the fluid viscosity in equation (54). It can be seen that our effective viscosity is a special case of equation (54) when the effect of fluid shear viscosity on compaction can be ignored.

Effective viscosities given by *Mckenzie* [1984], *Spiegelman et al*. [2001], *Stevenson and Scott* [1991], and *Sumita et al*. [1996] differ from the above result and from each other. *Mckenzie* [1984] refers to the microscopic model of *Arzt et al*. [1983] for hot isostatic pressing of metal powders, which assumes that during compaction, initially spherical particles become tetrakaidecahedrons tightly pressed to each other. Spherical pores remain at each vertex. Due to grain boundary diffusion, matter is transported from the contact between two particles to the surface of spherical voids; thus,

$$\eta_\varphi = \zeta^{\mathrm{x}} = \zeta_0 \frac{3\left(\varphi^{2/3} - 1\right) + \left(\varphi^{2/3} + 1\right) \ln 1/\varphi}{1 - \varphi^{2/3}} \tag{55}$$

where ζ_0 is constant depending on the atomic volume, grain boundary thickness, and grain boundary diffusion coefficient. However, due to poor experimental constraints on effective viscosity, *Mckenzie* [1984] assumes that $\eta_b = \zeta = const$, which gives

$$\eta_\varphi = \zeta^{\mathrm{x}} = \frac{\zeta_0}{1 - \varphi} \tag{56}$$

where ζ_0 is a constant reference viscosity. Following *Mckenzie* [1984], this expression for effective viscosity appears in *Mckenzie* [1987], *Richter and Mckenzie* [1984], and *Spiegelman* [1993]. *Stevenson and Scott* [1991] adopt

$$\eta_\varphi = \frac{\eta_s}{(1 - \varphi)\varphi^m} \tag{57}$$

where η_s is a constant reference viscosity, and m is a constant viscosity exponent. *Spiegelman et al*. [2001] use effective viscosity of the form

$$\eta_\varphi = \zeta_0 \frac{(\varphi_c/\varphi)^m + 4/3}{\varphi_c{}^m + 4/3} \tag{58}$$

where φ_c is a "compaction porosity" equal to a fraction of a reference porosity, e.g., $(0.1 - 0.5)\varphi_0$, and m is constant. *Sumita et al*. [1996] consider a spherical model for porous media similar to the one used in this paper. However, they come up with a different result:

$$\eta_\varphi = \frac{4}{3} \frac{1 - \varphi}{\varphi} \eta_s. \tag{59}$$

Takei and Katz [2013], based on a viscous contiguity model, give the following exponential expression for the effective viscosity in a texturally equilibrated partially molten rock:

$$\eta_b = 5/3 \eta_s \exp(-\lambda(\varphi - \varphi_0)) \tag{60}$$

with constants η_s, φ_0, and $\lambda \approx 27$.

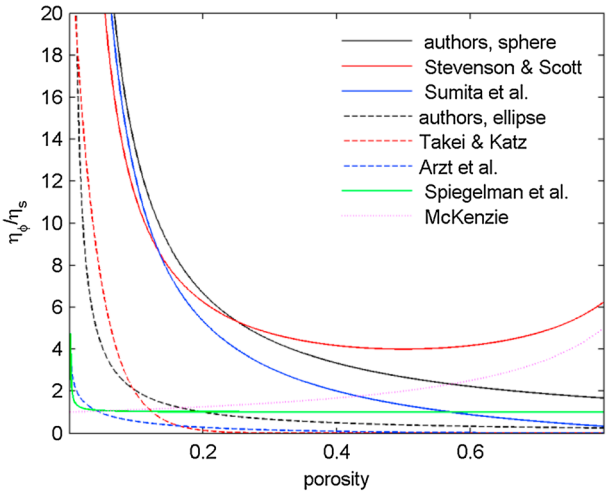

Figure 7. Compilation plot of selected effective viscosities.

Our effective viscosity in equation (24) obtained for cylindrical and spherical voids can be generalized to other pore geometries based on poroelastic model in equation (49) by using the viscoelastic correspondence principle:

$$\eta_\varphi = \widetilde{m}\frac{\eta_s}{\varphi} \tag{61}$$

where $\widetilde{m}$ is a geometric factor (see equation (48)). Figure 7 shows a comparison of various expressions for effective viscosity η_φ (expressions for η_b were converted using equation (52)). The curves include the effective viscosity in equation (61) obtained in this paper for spherical and elliptical pore geometries, the effective viscosity (equation (57)) of *Stevenson and Scott* [1991] with $m=1$, the viscosity (equation (59)) of *Sumita et al.* [1996], equation (58) from *Spiegelman et al.* [2001], the effective viscosity (equation (56)) given by *Mckenzie* [1984], the viscosity (equation (55)) from *Arzt et al.* [1983], and the viscosity (equation (60)) from *Takei and Katz* [2013]. It is interesting to note that while most of the models predict that effective viscosity decreases as φ increases, the models from *Mckenzie* [1984] and *Stevenson and Scott* [1991] show the opposite trends at high porosities. This might be explained by the ad hoc nature of equations (56) and (57). The major difference in equations (61), (57), and (59) is in the $1-\varphi$ factor. This factor is responsible for the deviation of the viscosities of *Sumita et al.* [1996] and *Stevenson and Scott* [1991] from our spherical trend. The deviation grows at higher values of φ (>0.25). Viscosity in equation (58) exhibits a rather weak dependence on parameters. Here we choose $\varphi_c = 0.5\varphi_0$, $m=3$, and $\varphi_0 = 0.01$. Our effective viscosity in equation (49) for elliptical pores with $\widetilde{m} = 0.2$ and the exponential viscosity from *Takei and Katz* [2013] give very similar predictions in a wide porosity range. At high porosities, the viscosity of *Arzt et al.* [1983] approaches these two. The difference between viscosities at small φ is mainly due to different assumptions on the pore geometry.

4.3. Poroplasticity

Only few theoretical models describe the rheology of compaction in complex nonlinear materials. Among them are the spherical models of *Carroll and Holt* [1972] for elastoplastic pore collapse and of *Wilkinson and Ashby* [1975] for compaction of composite powders by power law creep. *Carroll and Holt* [1972], based on considerations of the simple spherical shell, derived the pore compaction relation for elastic, elastoplastic, and fully plastic stages of compaction in porous materials with a pressure-insensitive von Mises type of plasticity. Our modeling reproduces the compaction relation of *Carroll and Holt* [1972] in a purely plastic regime in the case of pressure-insensitive plasticity and the porosity equation of *Wilkinson and Ashby* [1975] and *Carroll* [1980a] for purely viscous compaction. The critical pressures for the onset of pore collapse due to pressure-insensitive plasticity predicted by our model are the same as in *Carroll* [1980a]. At the same time, our model is a generalization of Carroll's elastoplastic model. Our model includes viscosity effects and incorporates two additional types of plasticity due to Mohr-Coulomb failure and Griffith fracturing. Viscoplastic models of compaction were developed in the works of *Wilkinson and Ashby* [1975], *Fischmeister et al.* [1978], and *Storakers et al.* [1999]. However, these models were primarily designed for industrial applications of powder compaction and deal with initial stages of compaction when particles are still disaggregated. Classical viscoplastic models were primarily designed for nonporous materials and do not include effect of porosity [*Chaboche*, 2008]. Our model includes effects of hardening/softening due to compaction and unlike most viscoplastic models accounts for the viscous deformation below the yield stress.

5. Comparison to Experiments

Empirical compaction relations for the brittle elastoplastic regime are frequently reported in the literature [*Wong and Baud*, 2012]. It is widely accepted that the initial elastic stages of compaction can be well

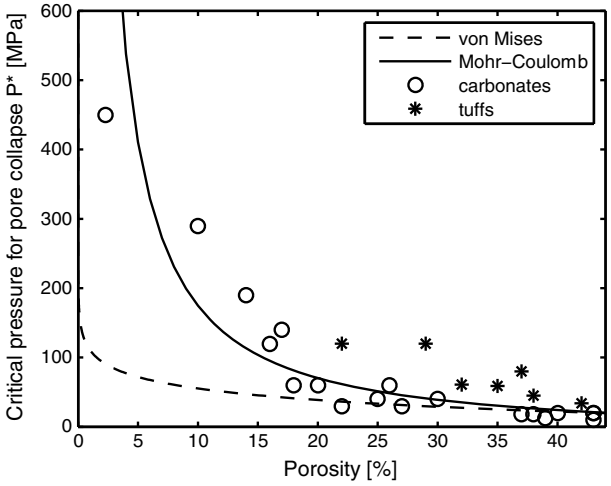

Figure 8. Comparison of theoretical predictions with laboratory data for critical pressures for pore collapse in carbonate rocks and tuffs [*Wong and Baud*, 2012].

described by an exponential law $\varphi = \varphi_0 \exp(\beta(p_0 - p_e))$ [*David et al*., 1994; *Dong et al*., 2010; *Zimmerman*, 1991], which results from the integration of the elastic part of our porosity equation (6) with effective bulk modulus equation (49) ($\beta = 1/\widetilde{m}G$). For sandstones, β is usually in the range between 0.44×10^{-3} MPa^{-1} and 3.30×10^{-3} MPa^{-1}, while for shales $\beta = (0.41 \text{ to } 1.30) \times 10^{-3}$ MPa^{-1} [*Dong et al*., 2010]. Assuming that the shear modulus of pure quartz, which is one of the major minerals forming sandstones, is $G = 31$ GPa; these data lead to $\widetilde{m}$ between 0.01 and 0.08. According to equation (48), such values would correspond to elliptic pores with aspect ratios between 0.007 and 0.05. However, with increasing effective pressure crack-like pores tend to close. Accordingly, $\widetilde{m}G$ is increasing, reflecting the fact that at higher pressures a cylindrical or spherical model becomes more appropriate.

In the fully plastic regime, our model for pressure-insensitive yielding in equation (29) coincides with the model of *Carroll and Holt* [1972], which was able to successfully predict the experimental data for a 38% porous tuff and 22% porous aluminum [*Carroll*, 1980a]. *Baud et al*. [2000] and *Vajdova et al*. [2004] showed that the same spherical model produces the best fit to the experimental data for the onset of pore collapse in porous carbonate rocks. In the linear viscous limit, our model coincides with the model of *Wilkinson and Ashby* [1975] for compaction by power law creep. This nonlinear model showed good agreement with measurements of the hot pressing of CoO powders. In rocks, most of the measurements focus on effective shear viscosity, while data on effective bulk viscosity is very scarce. However, all end-members of our model (elastic, viscous, and plastic) have good experimental support, which support confidence in the full model. Moreover, elastoplastic counterparts of our viscoplastic equations were able to reproduce low-temperature data from *Wong and Baud* [2012] for pore collapse in sandstone (Figure 8). We used our cylindrical model to describe the laboratory-measured dependence of the critical pore collapse pressure on porosity in carbonate rocks and tuffs presented by *Vajdova et al*. [2012] and *Wong and Baud* [2012]. In our model, critical pore collapse pressure is presented as an upper bound in equations (25) and (30) for pressure-insensitive and dilatant deformation, respectively. For pressure-insensitive plasticity, yield stress was set to $Y = 24$ MPa. For dilatant failure, cohesion is $Y = 8$ MPa, and the internal angle of friction is $\phi = 32,7°$. Pressure-insensitive yield (dashed line) significantly underestimates critical pressures for porosities below 18%, while the brittle failure model (black line) is able to reproduce critical pressures for the onset of pore collapse with a single curve that has just two well-constrained parameters.

6. Conclusions

Model results discussed in this paper belong to two very different parts. The first part deals with fundamental results, independent of pore geometry, that describe the general mathematical structure of the constitutive closure relationships, and the second part summarizes the most important findings of the pore-scale models and micro-macro schemes responsible for effective media theory derivations of bulk compressibility and viscosity coefficients that appeared in the first part as some unspecified positive coefficients. The independence of any assumptions about pore geometry of the first part of the paper constrains the general structure of the mathematical model. The proposed porous viscoelastoplastic model intends to predict three-dimensional behavior of fluid-rock systems during sedimentary compaction as well as during magmatic and metamorphic differentiation processes. We aimed at an increased level of coherence in the mathematical principles behind porous rock deformation. Our unifying mathematical model can be used in modeling of fluid and melt extraction from the solid Earth at a wide range of temperatures and time scales. The model is based on rigorous thermodynamic modeling so that the first and second laws of thermodynamics are enforced. Our thermodynamic

formulation provides the closure porosity equation, which is essential for compaction modeling. Other closure relationships are obtained from the basic principles of continuum mechanics. We used the mathematical similarity of purely elastic and purely viscous descriptions for nonporous materials known as the viscoelastic correspondence principle and ensured that such similarity still holds for porous viscoelastic materials. Our poroelastic constitutive equations are consistent with pore geometry-independent Gassmann's relations and the exact effective stress law, and they lead to Biot's equations in the linear limit. The source of disagreement between poroelastic constitutive equations by *Biot* [1956a] and the True Porous Media theory [*de Boer*, 2000; *Ehlers and Eipper*, 1999], which casted doubts on the validity of Biot's theory, is clarified.

In the second part, the effective elastic bulk modulus and effective pressure- and porosity-dependent bulk viscosity are obtained from the interpretation of the microstructure. We approximated the porous solid as an assembly of noninteracting pores with cylindrical or spherical geometry. We show that pressure-insensitive plastic flow around heterogeneities in viscoplastic rocks leads to an effective exponential creep law. If brittle permanent deformation accompanies viscous flow at the pore scale, the macroscopic rock behavior exhibits compaction-decompaction asymmetry. This asymmetry has been shown to cause the formation of a channeling instability in ductile porous media that provides a potential mechanism for effective transport in rocks [*Connolly and Podladchikov*, 2007; *Raess et al*., 2014].

Appendix A: Thermodynamic Derivation of Poroviscoelastoplastic Equations for Porous Media

A1. Local Balance Equations

In our description of porous materials we follow the formulation and recipes of classical irreversible thermodynamics [*Jou et al*., 2001]. We consider porous material as a two-phase system consisting of solid and fluid phases in which exchange of heat, momentum, and matter between the phases is possible. The balance equations for mass, momentum, entropy, and energy for the individual phase in the Euler representation are given by, e.g., *Gyarmati* [1970] and *Jou et al*. [2001]

$$\frac{\partial(\rho\varphi)}{\partial t}+\nabla_j\left(\rho\varphi v_j+q_\rho^j\right)=Q_\rho \tag{A1}$$

$$\frac{\partial(\rho\varphi v_i)}{\partial t}+\nabla_j\left(\rho\varphi v_i v_j+q_v^{ij}\right)=Q_{v_i} \tag{A2}$$

$$\frac{\partial(\rho\varphi s)}{\partial t}+\nabla_j\left(\rho\varphi s v_j+q_s^j\right)=Q_s \tag{A3}$$

$$\frac{\partial(\rho\varphi e)}{\partial t}+\nabla_j\left(\rho\varphi e v_j+q_e^j\right)=Q_e \tag{A4}$$

where ρ is the true density of an individual phase (mass of a phase in a unit volume of the same phase); φ is a volume fraction of a phase in a mixture; v_j, e, and s are specific values of velocity, total energy, and entropy referred to per unit mass, respectively; and ∇_j is the component of the del operator. Quantities q_ρ^j, q_v^{ij}, q_s^j, q_e^j and Q_ρ, Q_{v_i}, Q_s, Q_e represent fluxes and production rates of mass, momentum, entropy, and total energy, respectively. Einstein summation convention on repetitive indexes is adopted. Equations (A1)–(A4) must be written for every individual phase of a mixture. Indexes referring to a particular phase are omitted whenever we consider this phase independently from the other ones, and they appear explicitly when we deal with interactions between different phases. In the following we put $q_\rho^j=0$ to imply a particular choice of macroscopic velocity, v_j, as an appropriate barycentric averaging scheme of an unknown microscopic velocity field.

A2. Local Equilibrium Hypothesis in a Weak Formulation

Following the recipe of classical irreversible thermodynamics, we assume a local thermodynamic equilibrium relationship between the infinitesimal increment of the specific internal energy u for each phase and increments of specific entropy s, specific volume ρ, the equilibrium (elastic) part of phase volume fraction (porosity) φ^e along the system trajectory, and the equilibrium (elastic) part of the deviatoric strain rate $\dot{\varepsilon}_{ij}^e$, namely,

$$\frac{\mathrm{du}}{\mathrm{dt}}=gv_z+T\frac{\mathrm{ds}}{\mathrm{dt}}-p\frac{d(1/\rho)}{\mathrm{dt}}+\frac{1}{\rho}\tau_{ij}\dot{\varepsilon}_{ij}^e+\frac{\tau}{\rho\varphi}\frac{d\varphi^e}{\mathrm{dt}} \tag{A5}$$

where T, p, τ_{ij}, and τ are conjugate thermodynamic variables associated with entropy, density, strain rate, and volume fraction φ, respectively. Specific quantities are introduced per unit mass. The term $g v_z$ is due to gravitational potential energy. This formulation of local thermodynamic equilibrium for the solid and fluid phases only is weaker than the Biot's classical assumption on existence of internal energy potential of the total two-phase system for the linear poroelastic case.

A3. Thermodynamic Constraints on Fluxes and Productions

So far, we have not made any assumptions about the fluxes and productions in balance equations (A1)–(A4). In order to obtain thermodynamic constraints on the fluxes and production terms, we substitute the balance laws for mass, momentum, entropy, and energy in equations (A1)–(A4) into local thermodynamic equilibrium in equation (A5) and solve the latter with respect to the entropy production Q_s obtaining

$$TQ_s = T\nabla_j q_s^j - \Phi Q_\rho - v_i\left(Q_{v_i} - \nabla_j q_v^{ij}\right) + Q_e - \nabla_j q_e^j - \varphi\varepsilon_{ij}^e\tau_{ij} + p\varphi\nabla_j v_j - \rho g\varphi v_z + p\dot{\varphi} - \tau\dot{\varphi}^e \tag{A6}$$

where $\Phi = u + p/\rho - Ts - v_i v_i/2$ is the specific Gibbs free energy introduced here merely as a shorthand notation. The equation (A6) gives the so-called noncompensated heat production rate, i.e., energy dissipation for a given phase per unit volume and unit time. Entropy production in multiphase media can arise from interaction between the phases, interaction of the whole mixture with surroundings, and from the internal dissipative processes within each phase. We decompose entropy production into two parts, namely, $Q_s = Q_{s,\mathrm{intra}} + Q_{s,\mathrm{inter}}$. The first of them, $Q_{s,\mathrm{intra}}$, is the intraphase part of the entropy production defined by heterogeneities locally existing in a phase. These heterogeneities arise from spatial nonhomogeneous distributions of velocities, temperatures, densities, and so on and yield to gradients of thermodynamic fluxes of velocity, entropy, temperature, etc. The internal part of entropy production is the sum of the products of thermodynamic fluxes and the corresponding thermodynamic forces:

$$TQ_{s,\mathrm{intra}} = T\nabla_j q_s^j + v_i\nabla_j q_v^{ij} - \nabla_j q_e^j - \varphi\varepsilon_{ij}^e\tau_{ij} + p\varphi\nabla_j v_j - \rho\varphi g v_z \tag{A7}$$

The second, the interphase part of entropy production, $Q_{s,\mathrm{inter}}$, is a result of interaction of different phases of a mixture. For each phase, $Q_{s,\mathrm{inter}}$ is the sum of the products of the thermodynamic sources and forces

$$TQ_{s,\mathrm{inter}} = -\Phi Q_\rho - v_i Q_{v_i} + Q_e + p\dot{\varphi} - \tau\dot{\varphi}^e. \tag{A8}$$

The second law of thermodynamics requires that entropy production of the whole system is nonnegative, i.e., $\sum_{\mathrm{phases}} Q_s = \sum_{\mathrm{phases}} \left(Q_{s,\mathrm{intra}} + Q_{s,\mathrm{inter}}\right) \geq 0$. This is guaranteed if both the intraphase and the interphase parts of the entropy production of a mixture are nonnegative.

A3.1. Constitutive Equations for Fluxes

The intraphase entropy productions $Q_{s,\mathrm{intra}}$ are independent for each phase and therefore must be nonnegative for every phase regardless of phase interactions. The latter is assured if [e.g., *Müller and Müller* [2009], chapter 12]

$$q_s^j = -\lambda\nabla_j T/T \tag{A9}$$

$$q_e^j = Tq_s^j + v_i q_v^{ij} - v_z\hat{z}^j\int_0^z g\rho\varphi dz \tag{A10}$$

$$q_v^{ij} = -\varphi\tau_{ij} + \varphi p\delta_{ij} + \hat{z}^i\hat{z}^j\int_0^z g\rho\varphi dz. \tag{A11}$$

Equation (A9) is the Fourier law of heat conduction, providing that T has the meaning of absolute temperature, and λ is the heat conduction coefficient. Equation (A10) is analogous to the first law of thermodynamics for mixtures and states that the flux of the total energy is equilibrated by the heat flux, the mechanical dissipation, and the work against the gravitational force. Equation (A11) defines additive decomposition of the momentum fluxes into the partial deviatoric stresses τ_{ij} acting on a given phase, the pressures, and the stress due to the gravity. The following choice of the nonequilibrium part of the deviatoric strain rate

$$\varepsilon_{ij}^v = \varepsilon_{ij} - \varepsilon_{ij}^e = \tau_{ij}/(2\eta)$$

gives a Maxwell type of viscoelastic behavior for the shear mode. Here η is the shear viscosity of a given phase. Summarizing results in equations (A9)–(A11), the intraphase part of the entropy production takes the form

$$TQ_{s,\mathrm{intra}} = \frac{\lambda}{T}\left|\nabla_j T\right|^2 + \frac{\varphi}{2\eta}\sum_{i,j}{\tau_{ij}}^2. \tag{A12}$$

$Q_{s,\mathrm{intra}}$ is nonnegative if the heat conduction coefficient, and the viscosities are nonnegative.

A3.2. Restrictions on Productions

The interphase entropy productions $Q_{s,\mathrm{inter}}$ reflect interactions between the phase in question and other phases of the system and may be positive or negative. If there is no heat and matter exchange with the surroundings of the entire fluid-rock system, then the total entropy production due to interphase interactions within the mixture must be nonnegative, i.e., $\sum_{\mathrm{phases}} Q_{s,\mathrm{inter}} \geq 0$. Up to this point we did not specify the number and nature of the phases in a mixture; all the equations were written for a single phase. However, our main interest here is a description of fully saturated (or dry) porous materials, and therefore from now on we consider two-phase systems consisting of a fluid and a solid. We shall explicitly use superscripts "*f*" and "*s*" when referring to the fluid or solid phase, respectively. At fully saturated conditions $\varphi^f + \varphi^s = 1$, and the volume fraction of a fluid phase is a usual porosity, which we denote further as φ, so that $\varphi^f \equiv \varphi$ and $\varphi^s \equiv 1 - \varphi$. Conservation laws require that there is no net production of mass, momentum, and energy in a closed two-phase system; therefore, in equations (A1)–(A4), we must set $Q^f_\rho = -Q^s_\rho \equiv Q_\rho$, $Q^f_{v_i} = -Q^s_{v_i} \equiv Q_{v_i}$, and $Q^f_e = -Q^s_e \equiv Q_e$. Then, interphase entropy production becomes

$$\sum_{\mathrm{phases}} Q_{s,\mathrm{inter}} = -\left[\frac{\Phi}{T}\right]Q_\rho + \left[\frac{1}{T}\right]Q_e - \left[\frac{v_i}{T}\right]Q_{v_i} + \sum_{\mathrm{phases}}\left(\frac{p}{T}\frac{\mathrm{d}\varphi}{\mathrm{d}t} - \frac{\tau}{T}\frac{\mathrm{d}\varphi^e}{\mathrm{d}t}\right) \tag{A13}$$

where $[b] = b^f - b^s$, and d/dt denotes the material time derivative with respect to the relevant phase.

In the following we assume equilibrium mass and energy exchange between the phases, which requires corresponding terms of the interphase entropy production to be set to zero. This assumption is not essential but greatly simplifies the algebraic expressions for the following derivations. The input from Q_e in equation (A13) may be eliminated by making a common assumption that temperature variations are sufficiently slow and that there is no temperature jump between the phases, i.e., $T = T^f = T^s$ [*Bercovici et al.*, 2001; *Mckenzie*, 1984]. Mass exchange, Q_ρ, may be eliminated by assuming that $[\Phi] = 0$. We assume additive decomposition of porosity increments into elastic and dissipative parts, which together with the negativity of entropy production requires that inelastic porosity equation takes the form

$$\frac{\mathrm{d}^s\varphi}{\mathrm{d}t} - \frac{\mathrm{d}^s\varphi^e}{\mathrm{d}t} = -\frac{p_e}{\eta_\varphi} \tag{A14}$$

where $p_e = \overline{p} - p^f$ is the effective pressure, and η_φ is an effective viscosity. Note that thermodynamics allows several different definitions of effective viscosity, which would relate either effective pressure p_e or differential pressure $p^s - p^f$ to porosity changes.

With the assumptions made, the interphase entropy production becomes

$$\sum_{\mathrm{phases}} Q_{s,\mathrm{inter}} = \frac{[p-\tau]}{T}\frac{\mathrm{d}^s\varphi^e}{\mathrm{d}t} + \left(p^f\nabla_i\varphi - \tau^f\nabla_i\varphi^e - Q_{v_i}\right)\frac{[v_i]}{T} + \frac{[p]^2}{T\eta_\varphi}(1-\varphi). \tag{A15}$$

Equilibrium porosity compaction is associated with zero entropy production, which requires $[p - \tau] = 0$. We consider fluids that do not depend on the shape of the pore space containing them, and therefore the local equilibrium equation (A5) for the fluid phase should not contain the porosity term, i.e., $\tau^f = 0$. Under this assumption, the condition $[p - \tau] = 0$ converts to $\tau^s = p^s - p^f$. Finally, if we ignore relative accelerations between the phases and other dynamic effects, entropy producing momentum exchange can be chosen in the form

$$Q_{v_i} = p^f\nabla_i\varphi - \beta[v_i] \tag{A16}$$

that appears in a number of previous studies [*de Boer*, 2000; *Mckenzie*, 1984]. Thus, the total entropy production becomes

$$TQ_s = \frac{\lambda}{T}\left|\nabla_j T\right|^2 + \frac{1-\varphi}{2\eta_s}\sum_{i,j}\left(\tau^s_{ij}\right)^2 + \frac{\varphi}{2\eta_f}\sum_{i,j}\left(\tau^f_{ij}\right)^2 + \beta[v_i]\cdot[v_i] + \frac{p_e^2}{\eta_\varphi(1-\varphi)}. \tag{A17}$$

Entropy production is nonnegative if the coefficient of momentum exchange β and the effective viscosity are both nonnegative. The main achievement here is not only the nonnegativity of viscosity, but the demonstration that the choice of positive viscosity is sufficient to guarantee the nonnegative entropy production. Omitting factors like (1-φ) or φ in the solid density evolution equation would result in such an expression for the entropy production that would not be possible to make nonnegative by any choice of viscosity.

Appendix B: Calibration of the Poroelastic Model Versus Exact Results

B1. Calibration of Poroelastic Model Parameters Versus Gassmann's Equation

Equations (9) and (10) represent a pure compliance formulation. The stiffness formulation for the poroelastic volumetric deformation is as follows:

$$\frac{d\overline{p}}{dt} = -K_u\left(\nabla_k v_k^s + B\nabla_k q_k^D\right) \tag{B1}$$

$$\frac{dp_f}{dt} = -BK_u\left(\nabla_k v_k^s + \frac{1}{\alpha}\nabla_k q_k^D\right) \tag{B2}$$

where

$$K_u = \frac{K_d}{1-\alpha B}. \tag{B3}$$

Equations (9) and (B2) give physical meaning to the introduced moduli K_d and K_u as drained (p^f = const) and undrained ($\nabla_k q_k^D = 0$) bulk moduli, respectively;

$$K_d = -\frac{1}{\nabla_k v_k^s}\left.\frac{d\overline{p}}{dt}\right|_{p^f=\text{const}} \tag{B4}$$

$$K_u = -\frac{1}{\nabla_k v_k^s}\left.\frac{d\overline{p}}{dt}\right|_{\nabla_k q_k^D=0} \tag{B5}$$

in full agreement with classical definitions. Substitution of equations (12) and (13) into equation (B3) leads to the following relationship between K_d and K_u

$$K_u = K_d + \frac{\left(1-\frac{K_d}{K_s}\right)^2}{\frac{\varphi}{K_f}+\frac{1-\varphi}{K_s}-\frac{K_d}{K_s^2}}. \tag{B6}$$

The latter is a well-known Gassmann's relation that holds for poroelastic media with a homogeneous and isotropic solid frame [*Gassmann*, 1951; *Guéguen and Boutéca*, 2004; *Mavko et al*., 1998; *Smith et al*., 2003]. Thus, our constitutive equations are consistent with the exact Gassmann's equation. Additionally, it can be shown that the effective bulk modulus K_φ is related to the effective dry rock pore space compressibility, defined by *Mavko et al*. [1998] as

$$\frac{1}{K_{\text{pore}}} = -\frac{1}{V_p}\left.\frac{\partial V_p}{\partial \overline{p}}\right|_{p^f=0}. \tag{B7}$$

The relationship between the two effective bulk moduli of pore space then becomes

$$\frac{1}{K_\varphi} = \frac{(1-\varphi)\varphi}{K_{\text{pore}}} - \frac{\varphi}{K_s}. \tag{B8}$$

Replacing K_ϕ in equation (11) with K_{pore}, we reproduce a well-known relation [*Mavko et al*., 1998; *Walsh*, 1965]:

$$\frac{1}{K_d} = \frac{1}{K_s} + \frac{\phi}{K_{\text{pore}}}. \tag{B9}$$

Identifying K_d and K_u, we notice that α introduced by equation (12) is in fact the Biot-Willis parameter, and B introduced by equation (13) is the Skempton's coefficient.

B2. Calibration of Poroelastic Model Parameters Versus Effective Stress Law

Newly introduced poroelastic constitutive equations can be independently validated by the effective stress law, which is another exact result of the theory of elasticity. The effective stress law states that the drained

bulk modulus of a porous rock can be obtained from the measurements done on a saturated sample if the effective pressure is used [*von Terzaghi*, 1923], i.e.,

$$K_d = -\frac{1}{\nabla_k v_k^s}\frac{dp_{\text{eff}}}{dt}\bigg|_{\text{undrained}} \tag{B10}$$

where

$$dp_{\text{eff}} = d\overline{p} - (1 - K_d/K_s)dp^f \tag{B11}$$

as was shown by *Garg and Nur* [1973] and *Nur and Byerlee* [1971]. It can be seen that the linear version of our constitutive in equation (9) is a simple reformulation of the two equations (B10) and (B11).

Appendix C: Elastic (Viscous) Deformation of Cylindrical and Spherical Pores

Following *Carroll and Holt* [1972], we consider a thick cylindrical or spherical shell with inner radius a and outer radius b as in Figure 1. Uniform pressure rates $\dot{\overline{p}}$ and $\dot{p}^f$ are specified at the external and internal boundaries of the elastic shell, respectively. For the viscous model, pressures $\overline{p}$ and p^f are prescribed. Dry conditions are reproduced when $p^f = 0$. In the case of the cylindrical cavity, plane strain conditions are fulfilled.

Imposed external loads produce axisymmetric deformation so that only radial velocity v_r is nontrivial, giving rise to radial and hoop components of strain rates within the RVE

$$\varepsilon_{rr} = \partial v_r/\partial r, \quad \varepsilon_{\theta\theta} = v_r/r \tag{C1}$$

Note that even though we assumed the absence of shear deformation on a macroscale, deviatoric stresses are still present on a pore scale. Stresses within the shell are governed by the force balance equation in the form

$$\partial\sigma_{rr}/\partial r + m(\sigma_{rr} - \sigma_{\theta\theta})/r = 0 \tag{C2}$$

where σ_{rr} and $\sigma_{\theta\theta}$ are radial and hoop stresses, and (r, θ) are polar coordinates within the RVE. The parameter m indicates the geometry of a pore so that $m = 1$ for cylindrical pores and $m = 2$ for spherical ones. For elastic solids, the relation between deformation and a stress state is given by the rate form of Hooke's law, namely,

$$\varepsilon_{rr} = \frac{1}{(m+1)^2 G K_s^*}\left(\dot{\sigma}_{rr}\left((2m-1)K_s^* + G\right) - \dot{\sigma}_{\theta\theta}\left((2m-1)K_s^* - mG\right)\right) \tag{C3}$$

$$\varepsilon_{\theta\theta} = \frac{1}{m(m+1)^2 G K_s^*}\left(\dot{\sigma}_{\theta\theta}\left((2m-1)K_s^* + m^2 G\right) - \dot{\sigma}_{rr}\left((2m-1)K_s^* - mG\right)\right) \tag{C4}$$

where $K_s^* = K_s + (2-m)G/3$. At the pore scale, we assume linear elasticity even though finite strains may be large. Integrating equations (C1)–(C4) together with boundary conditions, we obtain

$$v_r = -\frac{r}{(m+1)K_s^*}\frac{\dot{\overline{p}}b^{m+1} - \dot{p}^f a^{m+1}}{b^{m+1} - a^{m+1}} - \frac{1}{2mGr^m}\frac{(ab)^{m+1}}{b^{m+1} - a^{m+1}}\left(\dot{\overline{p}} - \dot{p}^f\right) \tag{C5}$$

$$\dot{\sigma}_{rr} = -\frac{\dot{\overline{p}}b^{m+1} - \dot{p}^f a^{m+1}}{b^{m+1} - a^{m+1}} + \frac{(ab)^{m+1}}{b^{m+1} - a^{m+1}}\frac{\dot{\overline{p}} - \dot{p}^f}{r^{m+1}} \tag{C6}$$

$$\dot{\sigma}_{\theta\theta} = -\frac{\dot{\overline{p}}b^{m+1} - \dot{p}^f a^{m+1}}{b^{m+1} - a^{m+1}} - \frac{(ab)^{m+1}}{b^{m+1} - a^{m+1}}\frac{\dot{\overline{p}} - \dot{p}^f}{mr^{m+1}}. \tag{C7}$$

Using the correspondence principle, a solution to the linear viscous problem can be obtained from the elastic solution, giving the following expressions for velocity:

$$v_r = -\frac{1}{2m\eta_s r^m}\frac{(ab)^{m+1}}{b^{m+1} - a^{m+1}}\left(\overline{p} - p^f\right) \tag{C8}$$

and stresses

$$\begin{aligned}\sigma_{rr} &= -\frac{\overline{p}b^{m+1} - p^f a^{m+1}}{b^{m+1} - a^{m+1}} + \frac{(ab)^{m+1}}{b^{m+1} - a^{m+1}}\frac{\overline{p} - p^f}{r^{m+1}}\\ \sigma_{\theta\theta} &= -\frac{\overline{p}b^{m+1} - p^f a^{m+1}}{b^{m+1} - a^{m+1}} - \frac{(ab)^{m+1}}{b^{m+1} - a^{m+1}}\frac{\overline{p} - p^f}{mr^{m+1}}\end{aligned} \tag{C9}$$

where we assumed that rock grains are viscously incompressible. As can be seen from equations (C5)–(C9), final solutions depend only on the ratio of two radii a/b; therefore, one of the radii can be chosen arbitrarily. Then, the second radius of the shell is determined by the porosity of the macroscopic rock volume, i.e., $\varphi = (a/b)^{m+1}$. In order to account for shear-enhanced compaction, nonisotropic analytical solutions for an isolated void can be used as is suggested in *Yarushina et al*. [2010] and *Yarushina and Podladchikov* [2007].

In the effective media theory that we use here to obtain macroscopic constitutive relations, it is assumed that macrostress is the volume average of the stress field within an RVE [*Christensen*, 1979], i.e.,

$$\overline{\sigma}_{ij} = \frac{1}{V}\int_V \sigma_{ij} dV \tag{C10}$$

where V is the volume of an RVE. For cylindrical (spherical) geometry considered here, $V = \frac{2m}{m+1}\pi b^{m+1}$. The macroscopic total pressure is thus related to microscopic stresses as

$$\overline{p} = -\frac{\overline{\sigma}_{kk}}{3} = -\frac{1}{3V}\int_V \sigma_{kk} dV = -\frac{1}{3V}\int_V \frac{\partial}{\partial x_j}\left(\sigma_{kj} x_k\right) dV = -\frac{1}{3V}\int_{\partial V} \sigma_{kj} x_k n_j dS \tag{C11}$$

where ∂V is the boundary of an RVE, and n_j are the components of the unit vector normal to ∂V. Summation over repetitive index k is assumed. Here we used the divergence theorem and identity $\sigma_{kk} = \frac{\partial}{\partial x_j}\left(\sigma_{kj} x_k\right)$. For a cylindrical problem, $\sigma_{zz} = (\sigma_{rr} + \sigma_{\theta\theta})/2$. With this in mind and using the fact that constant radial stress is prescribed at the boundary of RVE defined as $r = b$, macroscopic total pressure becomes

$$\overline{p} = -\frac{1}{(m+1)V}\int_{\partial V} r\sigma_{rr}\, dS = \frac{\sigma_{rr}|_{r=b}}{(m+1)V}\int_{\partial V} b dS = \sigma_{rr}|_{r=b}. \tag{C12}$$

Equation (C12) shows that total pressure has to be prescribed at the external boundary of an RVE as a boundary condition for radial stress.

Appendix D: Viscoplastic Deformation of Cylindrical and Spherical Pores

In porous materials, plastic yielding will concentrate around pores. For modeling of viscoplastic deformation, we consider the same spherical (cylindrical) model as before (Figure 1). Viscous deformation of the solid mineral grains is assumed to be incompressible. Before plastic flow is initiated, the deformation of the shell is viscous. It is defined by equations (C8) and (C9). When viscous stresses reach a certain yield criterion, a circular plastic domain of radius c starts to grow around the cavity (Figure 3). From that point, two different domains must be distinguished. In the plastic domain surrounding the cavity, stresses can be found independent of kinematics. Experiments show that the failure envelope in rocks is nonlinear and exhibits three distinct modes (Figure 2) [*Escartin et al*., 1997; *Hirth*, 2002; *Jaeger et al*., 2007]. At low confinement, failure is sensitive to the mean normal stress, while with increasing confinement, dependence on the normal stress decreases until failure is almost nondilatant. In the tensile region, which corresponds to generation and growth of tensile fractures, the failure envelope is closed with a cap. For mathematical simplicity, here we use a piecewise linear approximation of the real envelope that consists of the Mohr-Coulomb criterion for dilatant brittle failure, the von Mises (Tresca) criterion for nondilatant failure, and the vertical limiting line for tensile Griffith-type fracturing. Von Mises (Tresca) and Mohr-Coulomb criteria can be represented as follows [*Yu*, 2006]:

$$\sigma_{rr} - \kappa\sigma_{\theta\theta} = Y^* + (\kappa - 1)p^f. \tag{D1}$$

For pressure-insensitive deformation, $\kappa = 1$ and $Y^* = Y\xi$ are the yield limits for pure shear in the case of cylindrical pores and half of the yield limit for simple tension in the case of spherical voids. The parameter ξ indicates the sign of loading ($\xi = 1$ for compaction and $\xi = -1$ for decompaction). For dilatant failure, parameters κ and Y^* are expressed through cohesion Y and internal angle of friction ϕ of the rock mineral grains as follows:

$$\kappa = (1 - \xi\sin\phi)/(1 + \xi\sin\phi) \tag{D2}$$

$$Y^* = 2Y\xi\cos\phi/(1 + \xi\sin\phi). \tag{D3}$$

Tensile fracturing is initiated when the Griffith failure criterion is satisfied [*Jaeger et al.*, 2007; *Yarushina and Podladchikov*, 2010]:

$$\sigma_{\theta\theta} = Y - p^f. \tag{D4}$$

Here Y is the uniaxial tensile strength. In the plastic region, simultaneous solution of force balance equation (C2) and yield criterion in equation (D1) or equation (D4) gives

$$\sigma_{rr} = -p^f - 2mY\xi \ln r/a, \;\; \sigma_{\theta\theta} = -p^f - 2Y\xi(1 + m \ln r/a), \tag{D5}$$

for pressure-insensitive deformation,

$$\sigma_{rr} = -p^f + \frac{Y^*}{\kappa - 1}\left((a/r)^{m(1-1/\kappa)} - 1\right), \;\; \sigma_{\theta\theta} = -p^f + \frac{Y^*}{(\kappa - 1)\kappa}\left((a/r)^{m(1-1/\kappa)} - \kappa\right), \tag{D6}$$

for dilatant brittle deformation, and

$$\sigma_{rr} = -p^f + Y(1 - (a/r)^m) \tag{D7}$$

for microfracturing.

In the viscous region, one has to fulfill force balance in equation (C2), kinematical relationships in equation (C1), and Newton's viscous law, leading to

$$\begin{aligned} \sigma_{rr} &= A - (A + \overline{p})(b/r)^{m+1} \\ \sigma_{\theta\theta} &= A + \frac{A + \overline{p}}{m}(b/r)^{m+1} \\ v_r &= b\frac{A + \overline{p}}{2m\eta_s}(b/r)^m. \end{aligned} \tag{D8}$$

Across the viscoplastic boundary, stresses must be continuous, which allows us to determine the unknown A and the plastic radius c. For von Mises (Tresca) materials

$$A = -\overline{p} - \frac{2m}{m+1}Y^*\xi\varphi(c/a)^{m+1},$$

and the plastic radius is given by the solution to the equation

$$|p_e/Y| = 2m/(m+1) \cdot \left(1 + \ln (c/a)^{m+1} - \varphi(c/a)^{m+1}\right). \tag{D9}$$

For Mohr-Coulomb materials,

$$A = -\overline{p} - \frac{m}{m+1}\frac{Y^*\varphi}{\kappa}(c/a)^{1+m/\kappa},$$

and the equation for c reads

$$\frac{1 + m/\kappa}{m+1}(c/a)^{m(1/\kappa - 1)} + \frac{m}{m+1}\frac{\kappa - 1}{\kappa}\varphi(c/a)^{1+m/\kappa} = 1 - (\kappa - 1)\frac{p_e}{Y^*}. \tag{D10}$$

For materials with microfracturing,

$$A = \frac{\overline{p}}{1 + \varphi(c/a)^{m+1}} - \varphi\frac{p^f - Y}{(c/a)^{-m-1} + \varphi}$$

where c can be found from equation

$$m(c/a)^{m+1}\varphi - (m+1)(1 + p_e/Y)(c/a)^m + 1 = 0 \tag{D11}$$

The velocity distribution in the plastic domain is found from the plastic flow rule, and the assumption on additive decomposition of the total strain rate, ε_{ij}, into plastic and viscous parts

$$\varepsilon^p_{rr}/\varepsilon^p_{\theta\theta} = \left(\varepsilon_{rr} - \varepsilon^v_{rr}\right)/\left(\varepsilon_{\theta\theta} - \varepsilon^v_{\theta\theta}\right) = -m/\varsigma \tag{D12}$$

where $\varsigma = 1$ for Tresca and von Mises materials and

$$\varsigma = (1 - \xi \sin\psi)/(1 + \xi \sin\psi) \tag{D13}$$

for Mohr-Coulomb friction. For Griffith material, we use the simplifying assumption that the generation of new fractures does not contribute to the volume change, in which case $\varsigma = 1$ in equation (D12). Substitution of viscous strain rates by stresses in equation (D12) according to Newton's law results in

$$\varsigma \frac{\partial v_r}{\partial r} + m \frac{v_r}{r} = \frac{\varsigma - 1}{(5 - m)\eta_s}(\sigma_{rr} - \sigma_{\theta\theta}).$$

Integration of this equation gives a radial velocity of the form

$$v_r = -\frac{Y^* \xi}{(m+1)\eta_s} \frac{c^{m+1}}{r^m} \qquad (r \le c) \tag{D14}$$

for pressure-insensitive materials ($\varsigma = 1$) and

$$v_r = -\frac{Y^* (a/r)^{m(1-1/\kappa)} r}{2(m+1)\kappa^2 \gamma \eta_s} ((c/r)^\gamma (\kappa + m) + (\gamma - 1)\kappa - m) \qquad (r \le c) \tag{D15}$$

for dilatant brittle deformation. Here

$$\gamma = 1 + (1/\kappa + 1/\varsigma - 1)m. \tag{D16}$$

During microfracturing, velocity in the plastic zone is given by equation (D8) due to assumed incompressibility. Viscoplastic deformation will continue as long as the plastic zone does not occupy the entire domain. The moment this happens corresponds to the full plastic pore collapse. Conditions for critical pressures at which this happens can be found from equations (D9) and (D10) by putting $c = b$.

Acknowledgments

We are grateful to Harro Schmeling, Einat Aharonov, Nina Simon, and Ludovic Räss for their helpful discussions and comments. We also acknowledge helpful reviews from Ives Guéguen, Francois Renard, and John Wheeler that improved the quality of the paper. This work is purely theoretical and makes no use of any specific data other than standard mathematical models described above. All the results of the paper can be reproduced following derivations specified in the text of the paper. This work was supported in part by a grant (193825/S60) from the Norwegian Research Council and IFE's strategic funds.

References

Arzt, E., M. F. Ashby, and K. E. Easterling (1983), Practical applications of hot-isostatic pressing diagrams - 4 case studies, *Metall. Mater. Trans. A*, *14*(2), 211–221.

Aydin, A., and A. M. Johnson (1983), Analysis of faulting in porous sandstones, *J. Struct. Geol.*, *5*(1), 19–31.

Baud, P., A. Schubnel, and T. F. Wong (2000), Dilatancy, compaction, and failure mode in Solnhofen limestone, *J. Geophys. Res.*, *105*(B8), 19,289–19,303, doi:10.1029/2000JB900133.

Bercovici, D., Y. Ricard, and G. Schubert (2001), A two-phase model for compaction and damage. 1. General Theory, *J. Geophys. Res.*, *106*(B5), 8887–8906, doi:10.1029/2000JB900430.

Berryman, J. G. (2005), Comparison of upscaling methods in poroelasticity and its generalizations, *J. Eng. Mech.*, *131*(9), 928–936, doi:10.1061/(Asce)0733-9399(2005)131:9(928).

Beuchert, M. J., and Y. Y. Podladchikov (2010), Viscoelastic mantle convection and lithospheric stresses, *Geophys. J. Int.*, *183*(1), 35–63, doi:10.1111/j.1365-246X.2010.04708.x.

Biot, M. A. (1941), General theory of three-dimensional consolidation, *J. Appl. Phys.*, *12*(2), 155–164.

Biot, M. A. (1956a), Theory of propagation of elastic waves in a fluid-saturated porous solid. 1. Low-frequency range, *J. Acoust. Soc. Am.*, *28*(2), 168–178.

Biot, M. A. (1956b), Theory of propagation of elastic waves in a fluid-saturated porous solid. 2. Higher frequency range, *J. Acoust. Soc. Am.*, *28*(2), 179–191.

Biot, M. A. (1962), Mechanics of deformation and acoustic propagation in porous media, *J. Appl. Phys.*, *33*(4), 1482–1498, doi:10.1063/1.1728759.

Budiansky, B., and R. J. Oconnell (1976), Elastic moduli of a cracked solid, *Int. J. Solids Struct.*, *12*(2), 81–97, doi:10.1016/0020-7683(76)90044-5.

Carroll, M. M. (1980a), Compaction of dry or fluid-filled porous materials, *J. Eng. Mech.*, *106*(5), 969–990.

Carroll, M. M. (1980b), Mechanical response of fluid-saturated porous materials, paper presented at XVth International Congress of Theoretical and Applied Mechanics, Amsterdam, New York, North-Holland Pub., Univ. of Toronto, Canada, 17–23 Aug.

Carroll, M. M., and A. C. Holt (1972), Static and dynamic pore-collapse relations for ductile porous materials, *J. Appl. Phys.*, *43*(4), 1626–1636.

Chaboche, J. L. (2008), A review of some plasticity and viscoplasticity constitutive theories, *Int. J. Plast.*, *24*(10), 1642–1693, doi:10.1016/j.ijplas.2008.03.009.

Christensen, R. M. (1979), *Mechanics of Composite Materials*, 348 pp., Wiley, New York.

Connolly, J. A. D., and Y. Y. Podladchikov (1998), Compaction-driven fluid flow in viscoelastic rock, *Geodin. Acta*, *11*(2–3), 55–84, doi:10.1016/S0985-3111(98)80006-5.

Connolly, J. A. D., and Y. Y. Podladchikov (2000), Temperature-dependent viscoelastic compaction and compartmentalization in sedimentary basins, *Tectonophysics*, *324*(3), 137–168.

Connolly, J. A. D., and Y. Y. Podladchikov (2007), Decompaction weakening and channeling instability in ductile porous media: Implications for asthenospheric melt segregation, *J. Geophys. Res.*, *112*, B10205, doi:10.1029/2005JB004213.

Connolly, J. A. D., and Y. Y. Podladchikov (2013), A hydromechanical model for lower crustal fluid flow, in *Metasomatism and the Chemical Transformation of Rock: The Role of Fluids in Terrestrial and Extraterrestrial Processes*, edited by D. E. Harlov and H. Austrheim, pp. 599–658, Springer, Berlin, doi:10.1007/978-3-642-28394-9.

Coussy, O. (1989), A general theory of thermoporoelastoplasticity for saturated porous materials, *Transp. Porous Media*, *4*(3), 281–293.

Coussy, O. (2004), *Poromechanics*, 2nd ed., 298 pp., Wiley, Chichester, U. K.

David, C., T. F. Wong, W. L. Zhu, and J. X. Zhang (1994), Laboratory measurement of compaction-induced permeability change in porous rocks: Implications for the generation and maintenance of pore pressure excess in the crust, *Pure Appl. Geophys.*, *143*(1–3), 425–456, doi:10.1007/Bf00874337.

de Boer, R. (2000), *Theory of Porous Media: Highlights in Historical Development and Current State*, 618 pp., Springer, Berlin.

Delacruz, V., P. N. Sahay, and T. J. T. Spanos (1993), Thermodynamics of porous media, *Proc. R. Soc. London, Ser. A*, *443*(1917), 247–255.

Detournay, E., and A. H. D. Cheng (1993), Fundamentals of poroelasticity, in *Comprehensive Rock Engineering: Principles, Practice and Projects*, edited by J. A. Hudson, pp. 113–171, Pergamon Press, Oxford, U. K.
Dong, J. J., J. Y. Hsu, W. J. Wu, T. Shimamoto, J. H. Hung, E. C. Yeh, Y. H. Wu, and H. Sone (2010), Stress-dependence of the permeability and porosity of sandstone and shale from TCDP Hole-A, *Int. J. Rock Mech. Min. Sci.*, *47*(7), 1141–1157, doi:10.1016/j.ijrmms.2010.06.019.
Duva, J. M., and J. W. Hutchinson (1984), Constitutive potentials for dilutely voided nonlinear materials, *Mech. Mater.*, *3*(1), 41–54.
Ehlers, W., and G. Eipper (1999), Finite elastic deformations in liquid-saturated and empty porous solids, *Transp. Porous Media*, *34*(1–3), 179–191, doi:10.1023/A:1006565509095.
Escartin, J., G. Hirth, and B. Evans (1997), Nondilatant brittle deformation of serpentinites: Implications for Mohr-Coulomb theory and the strength of faults, *J. Geophys. Res.*, *102*(B2), 2897–2913, doi:10.1029/96JB02792.
Evans, B., and C. Goetze (1979), Temperature variation of hardness of olivine and its implication for polycrystalline yield stress, *J. Geophys. Res.*, *84*(Nb10), 5505–5524, doi:10.1029/JB084ib10p05505.
Fischmeister, H. F., E. Arzt, and L. R. Olsson (1978), Particle deformation and sliding during compaction of spherical powders: Study by quantitative metallography, *Powder Metall.*, *21*(4), 179–187.
Fortin, J., Y. Gueguen, and A. Schubnel (2007), Effects of pore collapse and grain crushing on ultrasonic velocities and V-p/V-s, *J. Geophys. Res.*, *112*(B8), doi:10.1029/2005JB004005.
Frenkel, J. (1944), On tire theory of seismic and seismoelectric phenomena in a moist soil, *J. Phys.*, *8*(1–6), 230–241.
Garg, S. K., and A. Nur (1973), Effective stress laws for fluid-saturated porous rocks, *J. Geophys. Res.*, *78*(26), 5911–5921, doi:10.1029/JB078i026p05911.
Gassmann, F. (1951), Über die elastizität poröser medien, *Vierteljahrschrift Naturforsch. Ges. Zürich*, *96*, 1–23.
Goodier, J. N. (1936), Slow viscous flow and elastic deformation, *Philos. Mag.*, *22*(149), 678–681.
Gray, W. G., and C. T. Miller (2005), Thermodynamically constrained averaging theory approach for modeling flow and transport phenomena in porous medium systems: 1. Motivation and overview, *Adv. Water Resour.*, *28*(2), 161–180, doi:10.1016/j.advwatres.2004.09.005.
Green, R. J. (1972), Plasticity theory for porous solids, *Int. J. Mech. Sci.*, *14*(4), 215–224.
Guéguen, Y., and M. Boutéca (2004), *Mechanics of Fluid Saturated Rocks*, vol. xi, 450 pp., Elsevier Acad. Press, Amsterdam, Boston.
Guéguen, Y., L. Dormieux, and M. Boutéca (2004), Fundamentals of poromechanics, in *Mechanics of Fluid Saturated Rocks*, edited by Y. Guéguen and M. Boutéca, pp. 1–54, Elsevier Acad. Press, Amsterdam.
Gurevich, B. (2007), Comparison of the low-frequency predicitons of Biot's and de Boer's poroelasticity theories with Gassmann's equation, *Appl. Phys. Lett.*, *91*(9), doi:10.1063/1.2778763.
Gurson, A. L. (1977), Continuum theory of ductile rupture by void nucleation and growth. 1. Yield criteria and flow rules for porous ductile media, *J. Eng. Mater. Technol.-Trans. ASME*, *99*(1), 2–15.
Gyarmati, I. N. (1970), *Non-Equilibrium Thermodynamics. Field Theory and Variational Principles*, 184 pp., Springer, Berlin.
Hewitt, I. J., and A. C. Fowler (2008), Partial melting in an upwelling mantle column, *Proc. R. Soc. A*, *464*(2097), 2467–2491, doi:10.1098/rspa.2008.0045.
Hill, R. (1950), *The Mathematical Theory of Plasticity*, 356 pp., Clarendon Press, Oxford, U. K.
Hirth, G. (2002), Laboratory constraints on the rheology of the upper mantle, in *Plastic Deformation of Minerals and Rocks*, edited by S. Karato and H.-R. Wenk, pp. 97–120, Mineral. Soc. of Am., Washington, D. C.
Houlsby, G. T., and A. M. Puzrin (2000), A thermomechanical framework for constitutive models for rate-independent dissipative materials, *Int. J. Plast.*, *16*(9), 1017–1047.
Jaeger, J. C., N. G. W. Cook, and R. W. Zimmerman (2007), *Fundamentals of Rock Mechanics*, 4th ed., vol. xi, 475 pp., Blackwell, Malden, Mass.
Johnson, P. A., and P. N. J. Rasolofosaon (1996), Nonlinear elasticity and stress-induced anisotropy in rock, *J. Geophys. Res.*, *101*(B2), 3113–3124, doi:10.1029/95JB02880.
Jou, D., J. Casas-Vázquez, and G. Lebon (2001), *Extended Irreversible Thermodynamics*, 3rd ed., 462 pp., Springer, Berlin.
Kadish, A., P. A. Johnson, and B. Zinszner (1996), Evaluating hysteresis in Earth materials under dynamic resonance, *J. Geophys. Res.*, *101*(B11), 25,139–25,147, doi:10.1029/96JB02480.
Karato, S. (2008), *Deformation of Earth Materials: An Introduction to the Rheology of Solid Earth*, vol. x, 463 pp., Cambridge Univ. Press, Cambridge, New York.
Karcz, Z., E. Aharonov, D. Ertas, R. Polizzotti, and C. H. Scholz (2008), Deformation by dissolution and plastic flow of a single crystal sodium chloride indenter: An experimental study under the confocal microscope, *J. Geophys. Res.*, *113*, B04205, doi:10.1029/2006JB004630.
Keller, T., D. A. May, and B. J. P. Kaus (2013), Numerical modelling of magma dynamics coupled to tectonic deformation of lithosphere and crust, *Geophys. J. Int.*, *195*(3), 1406–1442, doi:10.1093/Gji/Ggt306.
Lopatnikov, S. L., and A. H. D. Cheng (2004), Macroscopic Lagrangian formulation of poroelasticity with porosity dynamics, *J. Mech. Phys. Solids*, *52*(12), 2801–2839, doi:10.1016/j.jmps.2004.05.005.
Lyakhovsky, V., and Y. Hamiel (2007), Damage evolution and fluid flow in poroelastic rock, *Izv. Phys. Solid Earth*, *43*(1), 13–23, doi:10.1134/S106935130701003x.
Lyakhovsky, V., Y. Podladchikov, and A. Poliakov (1993), A rheological model of a fractured solid, *Tectonophysics*, *226*(1–4), 187–198.
Lyakhovsky, V., Z. Reches, R. Weinberger, and T. E. Scott (1997), Non-linear elastic behaviour of damaged rocks, *Geophys. J. Int.*, *130*(1), 157–166.
Mackenzie, J. K. (1950), The elastic constants of a solid containing spherical holes, *Proc. Phys. Soc. London, Sect. B*, *63*(361), 2–11, doi:10.1088/0370-1301/63/1/302.
Mashinskii, E. I. (2003), The amplitude dependence of seismic wave velocities, *Izv. Phys. Solid Earth*, *39*(12), 992–998.
Mavko, G., T. Mukerji, and J. Dvorkin (1998), *The Rock Physics Handbook: Tools for Seismic Analysis in Porous Media*, 329 pp., Cambridge Univ. Press, Cambridge, New York.
Mckenzie, D. (1984), The generation and compaction of partially molten rock, *J. Petrol.*, *25*(3), 713–765.
Mckenzie, D. (1987), The compaction of igneous and sedimentary rocks, *J. Geol. Soc.*, *144*, 299–307.
Müller, I., and W. H. Müller (2009), *Fundamentals of Thermodynamics and Applications: With Historical Annotations and Many Citations From Avogadro to Zermelo*, vol. xvi, 404 pp., Springer, Berlin.
Nguyen, S. H., A. I. Chemenda, and J. Ambre (2011), Influence of the loading conditions on the mechanical response of granular materials as constrained from experimental tests on synthetic rock analogue material, *Int. J. Rock Mech. Min. Sci.*, *48*(1), 103–115, doi:10.1016/j.ijrmms.2010.09.010.
Nur, A., and J. D. Byerlee (1971), Exact effective stress law for elastic deformation of rock with fluids, *J. Geophys. Res.*, *76*(26), 6414–6419, doi:10.1029/JB076i026p06414.

Peng, Z. G., and J. Gomberg (2010), An integrated perspective of the continuum between earthquakes and slow-slip phenomena, *Nat. Geosci.*, *3*(9), 599–607, doi:10.1038/Ngeo940.
Perzyna, P., and A. Drabik (1989), Description of micro-damage process by porosity parameter for nonlinear viscoplasticity, *Arch. Mech.*, *41*(6), 895–908.
Pride, S. R., A. F. Gangi, and F. D. Morgan (1992), Deriving the equations of motion for porous isotropic media, *J. Acoust. Soc. Am.*, *92*(6), 3278–3290, doi:10.1121/1.404178.
Raess, L., V. M. Yarushina, N. S. C. Simon, and Y. Y. Podladchikov (2014), Chimneys, channels, pathway flow or water conducting features: An explanation from numerical modelling and implications for CO_2 storage, *Energy Procedia*, *63*, 3761–3774.
Rice, J. R. (1975), Stability of dilatant hardening for saturated rock masses, *J. Geophys. Res.*, *80*(11), 1531–1536, doi:10.1029/JB080i011p01531.
Rice, J. R., and M. P. Cleary (1976), Some basic stress diffusion solutions for fluid-saturated elastic porous media with compressible constituents, *Rev. Geophys.*, *14*(2), 227–241, doi:10.1029/RG014i002p00227.
Richter, F. M., and D. Mckenzie (1984), Dynamical models for melt segregation from a deformable matrix, *J. Geol.*, *92*(6), 729–740.
Schanz, M. (2009), Poroelastodynamics: Linear models, analytical solutions, and numerical methods, *Appl. Mech. Rev.*, *62*(3), doi:10.1115/1.3090831.
Schanz, M., and S. Diebels (2003), A comparative study of Biot's theory and the linear Theory of Porous Media for wave propagation problems, *Acta Mech.*, *161*(3–4), 213–235, doi:10.1007/s00707-002-0999-5.
Schmeling, H. (2000), Partial melting and melt segregation in a convecting mantle, in *Physics and Chemistry of Partially Molten Rocks*, edited by N. Bagdassarov, D. Laporte, and A. B. Thompson, pp. 141–178, Kluwer Acad. Publ., Dordrecht, Netherlands.
Schmeling, H., J. P. Kruse, and G. Richard (2012), Effective shear and bulk viscosity of partially molten rock based on elastic moduli theory of a fluid filled poroelastic medium, *Geophys. J. Int.*, *190*(3), 1571–1578, doi:10.1111/j.1365-246X.2012.05596.x.
Scott, D. R., and D. J. Stevenson (1984), Magma solitons, *Geophys. Res. Lett.*, *11*(11), 1161–1164, doi:10.1029/GL011i011p01161.
Sheldon, H. A., A. C. Barnicoat, and A. Ord (2006), Numerical modelling of faulting and fluid flow in porous rocks: An approach based on critical state soil mechanics, *J. Struct. Geol.*, *28*(8), 1468–1482, doi:10.1016/j.jsg.2006.03.039.
Sleep, N. H. (1974), Segregation of magma from a mostly crystalline mush, *Geol. Soc. Am. Bull.*, *85*(8), 1225–1232.
Smith, T. M., C. H. Sondergeld, and C. S. Rai (2003), Gassmann fluid substitutions: A tutorial, *Geophysics*, *68*(2), 430–440, doi:10.1190/1.1567211.
Sonder, L. J., and P. England (1986), Vertical averages of Rheology of the continental lithosphere - relation to thin sheet parameters, *Earth Planet. Sci. Lett.*, *77*(1), 81–90, doi:10.1016/0012-821x(86)90134-2.
Spiegelman, M. (1993), Physics of melt extraction: Theory, implications and applications, *Philos. Trans. R. Soc. London, Ser. A*, *342*(1663), 23–41.
Spiegelman, M., P. B. Kelemen, and E. Aharonov (2001), Causes and consequences of flow organization during melt transport: The reaction infiltration instability in compactible media, *J. Geophys. Res.*, *106*(B2), 2061–2077, doi:10.1029/2000JB900240.
Sramek, O., Y. Ricard, and D. Bercovici (2007), Simultaneous melting and compaction in deformable two-phase media, *Geophys. J. Int.*, *168*(3), 964–982, doi:10.1111/j.1365-246X.2006.03269.x.
Stevenson, D. J., and D. R. Scott (1991), Mechanics of fluid-rock systems, *Annu. Rev. Fluid Mech.*, *23*, 305–339.
Storakers, B., N. A. Fleck, and R. M. McMeeking (1999), The visco-plastic compaction of composite powders, *J. Mech. Phys. Solids*, *47*(4), 785–815.
Sumita, I., S. Yoshida, M. Kumazawa, and Y. Hamano (1996), A model for sedimentary compaction of a viscous medium and its application to inner-core growth, *Geophys. J. Int.*, *124*(2), 502–524.
Takei, Y., and R. F. Katz (2013), Consequences of viscous anisotropy in a deforming, two-phase aggregate. Part 1. Governing equations and linearized analysis, *J. Fluid Mech.*, *734*, 424–455, doi:10.1017/Jfm.2013.482.
Turcotte, D. L., and J. L. Ahern (1978), Porous flow model for magma migration in asthenosphere, *J. Geophys. Res.*, *83*, 767–772, doi:10.1029/JB083iB02p00767.
Tvergaard, V. (1981), Influence of voids on shear band instabilities under plane-strain conditions, *Int. J. Fract.*, *17*(4), 389–407.
Vajdova, V., P. Baud, and T. F. Wong (2004), Compaction, dilatancy, and failure in porous carbonate rocks, *J. Geophys. Res.*, *109*, B05204, doi:10.1029/2003JB002508.
Vajdova, V., P. Baud, L. Wu, and T. F. Wong (2012), Micromechanics of inelastic compaction in two allochemical limestones, *J. Struct. Geol.*, *43*, 100–117, doi:10.1016/j.jsg.2012.07.006.
von Terzaghi, K. (1923), Die berechnung der durchlassigkeit des tones aus dem verlauf der hydromechanischen spannungserscheinungen, *Sitzungsber. Akad. Wiss. Wien, Math.-Naturwiss. Kl.*, *132*, 125–138.
Walsh, J. B. (1965), Effect of cracks on compressibility of rock, *J. Geophys. Res.*, *70*(2), 381–389, doi:10.1029/JZ070i002p00381.
Wang, H. (2000), *Theory of Linear Poroelasticity With Applications to Geomechanics and Hydrogeology*, 287 pp., Princeton Univ. Press, Princeton, N. J.
Wilkinson, D. S., and M. F. Ashby (1975), Pressure sintering by power law creep, *Acta Metall.*, *23*(11), 1277–1285.
Wilmanski, K. (2006), A few remarks on Biot's model and linear acoustics of poroelastic saturated materials, *Soil Dyn. Earthquake Eng.*, *26*(6–7), 509–536, doi:10.1016/j.soildyn.2006.01.006.
Wong, T. F., and P. Baud (2012), The brittle-ductile transition in porous rock: A review, *J. Struct. Geol.*, *44*, 25–53, doi:10.1016/j.jsg.2012.07.010.
Yarushina, V. M., and Y. Y. Podladchikov (2007), The effect of nonhydrostaticity on elastoplastic compaction and decompaction, *Izv. Phys. Solid Earth*, *43*(1), 67–74, doi:10.1134/S1069351307010077.
Yarushina, V. M., and Y. Y. Podladchikov (2010), Plastic yielding as a frequency and amplitude independent mechanism of seismic wave attenuation, *Geophysics*, *75*(3), N51–N63, doi:10.1190/1.3420734.
Yarushina, V. M., M. Dabrowski, and Y. Y. Podladchikov (2010), An analytical benchmark with combined pressure and shear loading for elastoplastic numerical models, *Geochem. Geophys. Geosyst.*, *11*, Q08006, doi:10.1029/2010GC003130.
Yarushina, V. M., D. Bercovici, and M. L. Oristaglio (2013), Rock deformation models and fluid leak-off in hydraulic fracturing, *Geophys. J. Int.*, *194*(3), 1514–1526, doi:10.1093/Gji/Ggt199.
Yu, H.-S. (2006), *Plasticity and Geotechnics*, vol. xx, 522 pp., Springer, New York.
Zimmerman, R. W. (1991), *Compressibility of Sandstones*, 173 pp., Elsevier, New York.